Lempka Scott (Orcid ID: 0000-0003-0964-311X)

Title

Patient-specific analysis of neural activation during spinal cord stimulation for pain

Running Title

Patient-specific analysis of SCS

Authors' Names

Scott F. Lempka, PhD[1,2,3,4,5], Hans J. Zander, BBmE[3,5], Carlos J. Anaya, BS[3,5], Alexandria Wyant, BA[1], John G. Ozinga, IV, PA-C[1,6], Andre G. Machado, MD, PhD[1,6]

Institutional Affiliation

[1] Center for Neurological Restoration, Cleveland Clinic, Cleveland, OH, USA

[2] Research Service, Louis Stokes Cleveland Veterans Affairs Medical Center, Cleveland, OH, USA

[3] Department of Biomedical Engineering, University of Michigan, Ann Arbor, MI, USA

[4] Department of Anesthesiology, University of Michigan, Ann Arbor, MI, USA

[5] Biointerfaces Institute, University of Michigan, Ann Arbor, MI, USA

[6] Department of Neurosurgery, Neurological Institute, Cleveland Clinic, Cleveland, OH, USA

Source(s) of Financial Support

This work was supported by the National Institutes of Health (NIH R01 NS089530) (Hans J. Zander and Scott F. Lempka), the Louis Stokes Cleveland Veterans Affairs Medical Center,

Cleveland, OH, USA (Scott F. Lempka), the University of Michigan Rackham Merit Fellowship Program (Carlos J. Anaya), and the Cleveland Clinic Research Program Committees, Cleveland, OH, USA (Scott F. Lempka). This research was supported in part through computational resources and services provided by Advanced Research Computing at the University of Michigan, Ann Arbor, MI, USA.

Authorship Statements

All authors were responsible for the study concept and design. Scott F. Lempka and John G. Ozinga performed the data acquisition. Scott F. Lempka, Hans Zander, Carlos J. Anaya performed the model design. Scott F. Lempka performed the model analysis. Scott F. Lempka prepared the manuscript draft, figures, and table with guidance from Alexandria Wyant, John G. Ozinga, and Andre G. Machado. All authors provided intellectual input and assisted with manuscript revisions. All authors approved the final version of the manuscript.

Conflicts of Interest

Scott F. Lempka holds stock options with Presidio Medical, Inc. and serves on the scientific advisory board. Andre G. Machado has distribution rights to Cardionomic, Inc. and Enspire DBS, Inc., and is a paid consultant of St. Jude Medical. Hans J. Zander, Carlos J. Anaya, Alexandria Wyant and John G. Ozinga declare no competing interests.

Corresponding Author

Scott F. Lempka, Ph.D.

Department of Biomedical Engineering

University of Michigan

2800 Plymouth Road, NCRC 014-184

Ann Arbor, MI 48104-2800

(734) 764-2401

lempka@umich.edu

Objective: Despite the widespread use of spinal cord stimulation (SCS) for chronic pain management, its neuromodulatory effects remain poorly understood. Computational models provide a valuable tool to study SCS and its effects on axonal pathways within the spinal cord. However, these models must include sufficient detail to correlate model predictions with clinical effects, including patient-specific data. Therefore, the goal of this study was to investigate axonal activation at clinically-relevant SCS parameters using a computer model that incorporated patient-specific anatomy and electrode locations.

Methods: We developed a patient-specific computer model for a patient undergoing SCS to treat chronic pain. This computer model consisted of two main components: 1) finite element model of the extracellular voltages generated by SCS and 2) multi-compartment cable models of axons in the spinal cord. To determine the potential significance of a patient-specific approach, we also performed simulations with standard canonical models of SCS. We used the computer models to estimate axonal activation at clinically-measured sensory, comfort, and discomfort thresholds.

Results: The patient-specific and canonical models predicted significantly different axonal activation. Relative to the canonical models, the patient-specific model predicted sensory threshold estimates that were more consistent with the corresponding clinical measurements. These results suggest that it is important to account for sources of interpatient variability (e.g. anatomy, electrode locations) in model-based analysis of SCS.

Conclusions: This study demonstrates the potential for patient-specific computer models to quantitatively describe the axonal response to SCS and to address scientific questions related to clinical SCS.

Key Words: Spinal Cord Stimulation; Chronic Pain; Computer Simulation; Failed Back Surgery Syndrome

INTRODUCTION

Spinal cord stimulation (SCS) is a common neurostimulation therapy for neuropathic pain conditions (e.g. failed back surgery syndrome, complex regional pain syndrome) that are refractory to conventional treatments.[1–3] Although SCS has been a widely-used clinical therapy for decades, it still has limited success (~50% of patients receive ≥50% reduction in pain).[3]

To improve clinical outcomes of SCS, we need to better understand the electric fields generated by SCS and their direct effects on the nervous system.[4] While experimental and/or clinical studies are useful in studying the mechanisms of action of neurostimulation therapies,[4–8] these studies include shortcomings related to interspecifies differences and difficulties in assessing stimulation quality and perception in animal models. In the past, several groups have used computational models to study the bioelectric effects of SCS. These studies have helped improve lead design, stimulation configurations, waveform parameters, and programming procedures.[9–13] Computational models have also provided insight into the direct neural response to SCS and its potential mechanisms of action.[14–17]

Although these computational studies have been productive, they utilized canonical models with geometric parameters based on average anatomical measurements with the goal of investigating technical and scientific principles that could be generalized to the target patient population. Typically, these generalized models do not account for the interpatient variability in anatomy and electrode locations that has been previously reported.[18,19] Clinical experience indicates significant variability in the therapeutic stimulation parameters (e.g. amplitude, pulse width, stimulation configuration), lead placement, and the degree of efficacy across patients that may limit the utility or accuracy of canonical SCS models in predicting the neural response

within individual patients.[19–24] To successfully correlate model-based predictions with patient-specific clinical effects, it may be necessary for computer models of SCS to incorporate three-dimensional (3D) patient-specific anatomy and electrode locations. 3D patient-specific computational models have shown tremendous success in defining optimal stimulation parameters and describing potential mechanisms of action in other neurostimulation therapies, such as deep brain stimulation,[25–28] but they have never been applied to SCS.

Therefore, the goal of this study was to develop a 3D patient-specific computer model of SCS. We defined the patient-specific model from preoperative and postoperative imaging and electrode impedance measurements for a patient undergoing SCS to treat neuropathic pain. We performed clinical measurements to assess the subject's sensory, comfort, and discomfort thresholds across several sets of stimulation parameters (e.g. pulse width, stimulation configuration). We also compared the results derived from the patient-specific computer model to results predicted by canonical models of SCS.

METHODS

Patient demographics

This study was reviewed and approved by the institutional review board at the Cleveland Clinic (Cleveland, OH, USA). We recruited one patient who was being treated with SCS as part of his standard clinical care and who provided informed consent to participate in the study. The patient was a 37-year-old male who had been diagnosed with post-laminectomy syndrome with chronic pain in his left leg. Approximately two weeks prior to enrollment, a three-column paddle lead array (Medtronic Model 39565 Specify™ 5-6-5 Surgical Lead, Medtronic, Inc., Minneapolis,

MN) had been implanted at the T8-T9 spinal levels and connected to a rechargeable voltage-regulated implantable pulse generator (IPG) (RestoreSensor™ Model 37714, Medtronic, Inc.).

Clinical testing

We performed all clinical testing procedures at a single visit approximately 6 weeks after SCS implantation to allow time for encapsulation of the implanted electrode array.[29] To localize the electrode array relative to the spine, we obtained a postoperative computed tomography scan of the lower thoracic spinal levels (see 'Model Analysis'). We measured the sensory threshold (ST), comfort threshold (CT), and discomfort threshold (DT) for several sets of stimulation parameters. To determine these thresholds, we followed 5 steps: 1) we increased the amplitude until the participant experienced stimulation-induced paresthesias, 2) we reduced the amplitude until the participant no longer reported paresthesias, 3) we increased the amplitude in 0.1 V increments until the participant experienced paresthesias (defined as the ST), 4) we increased the amplitude until the stimulation became uncomfortable (defined as the DT), and 5) we decreased the amplitude until the stimulation-induced paresthesias were at a maximum intensity that was comfortable to the participant (defined as the CT).

To consider the effects of stimulation parameters on axonal recruitment, we varied the pulse width and the stimulation configuration.[10,12] For each set of stimulation parameters, we used a standard pulse frequency of 50 Hz.[30] We tested the following pulse widths: 60, 210, 300, 450, and 1000 μs. We tested the following stimulation configurations: bipole, longitudinal guarded cathode, transverse guarded cathode, and pseudo-monopole. We used a single cathode, which had provided the participant with significant pain relief (see the Supplemental

Methods, Supporting Information for further details). To help ensure that the spinal cord was in a similar position relative to the spine during both imaging procedures and clinical testing, we performed the testing procedures while the participant was supine on an exam bed.

Because the participant's commercial SCS system utilized voltage-controlled stimulation, we also considered the effects of electrode impedance on stimulation thresholds. At the end of the research testing, we measured the bipolar electrode impedances across the entire array. The average electrode impedance was 695±34.7 Ω.

Model analysis

Step 1: Calculate the extracellular voltages generated by SCS

The first step in our model analysis was to estimate the extracellular voltages generated in the spinal cord during SCS. We developed a finite element model (FEM) of the lower thoracic spinal cord and surrounding anatomy based on the patient-specific anatomy and electrode locations. We used preoperative magnetic resonance imaging (MRI) to segment the participant's spinal cord, cerebrospinal fluid (CSF), epidural fat, and spine (Fig. 1). We used the postoperative computed tomography scan to localize the SCS electrodes and segment the participant's spine. We then co-registered the segmented 3D surfaces from the preoperative and postoperative images and defined a patient-specific FEM. This patient-specific FEM included a spinal cord domain scaled to match the anteroposterior and mediolateral dimensions of the participant's spinal cord anatomy at the T9 spinal level and included an explicit representation of the electrode array. The FEM also included a domain to represent the electrode encapsulation that occurs with chronic SCS implants.[29] To assess whether or not

there is an advantage to the patient-specific approach compared to previously-used canonical models, we also performed simulations with two versions of a canonical FEM. In the first canonical FEM, the same SCS array was placed on the dural surface along the spinal cord midline to resemble previous canonical models of SCS.[16,20,31–33] The second canonical FEM was an "impedance-matched" model that, like the patient-specific FEM, included an additional domain to represent the electrode encapsulation.

We assigned electrical conductivities to each domain using experimental data available in the literature.[12,14,34] For the patient-specific and the impedance-matched FEMs, we adjusted the encapsulation layer conductivity until each FEM produced average electrode impedances that matched the clinical impedance measurements. We applied 1 V and 0 V boundary conditions at the cathode and anode(s), respectively, set the outer tissue boundary of the FEM to be perfectly insulating, and solved Laplace's equation. The corresponding spatially-dependent FEM voltage solutions were then scaled by the time-dependent output of the IPG to determine the spatiotemporal extracellular voltages generated by SCS.[35,36]

Step 2: Define axon models in the spinal cord

The next step was to define computer models of spinal cord axons. With regards to SCS, studies have shown that the two axon types most likely affected by SCS are the large-diameter myelinated dorsal root (DR) fibers and Aβ fibers within the dorsal columns (DC).[14,37] Therefore, we included computer models of both DR and DC fibers in our analysis (Fig. 2). We used a previously-published compartmental model of a mammalian axon[38] to represent these axons. For both patient-specific and canonical models, we generated axon populations within

the white matter boundaries of the spinal cord that covered a range of diameters (i.e. 5.7-11.5 μm) to match the axon diameters and densities measured in the DC of the human spinal cord.[37] We also defined DR fibers that had a 3D axon trajectory in which they entered the spinal cord at a 45-degree angle.[39] We placed DR fibers in 1 mm intervals along the rostrocaudal axis. Near the dorsal horn, the DR fiber branched into a daughter fiber that traveled along the rostrocaudal axis within the DC.

Step 3: Assess the axonal response to SCS

The final step was to assess the axonal response to SCS under each set of conditions in our patient-specific and canonical models. We applied the extracellular voltages defined by the FEM (Step 1) to the axon models (Step 2) (Fig. 3). We then calculated the activation thresholds and a model-predicted ST for each parameter set and compared these model estimates to the corresponding clinical ST, CT, and DT.

Activation threshold. We defined the activation threshold as the minimum pulse amplitude required to generate an action potential for each stimulus pulse in a particular axon.

Model sensory threshold. To compare our model predictions to our clinical measurements, we defined a model ST as the pulse amplitude required to activate ≥10% of the DC axons.[11]

Pulse width. We calculated the model ST for each pulse width that we tested clinically: 60, 210, 300, 450, and 1000 μs.

Stimulation configuration. We calculated the activation thresholds and model ST for each stimulation configuration that we tested clinically: bipole, longitudinal guarded cathode, transverse guarded cathode, pseudo-monopole.

For a complete description of the model development and analysis, see the Supplemental Methods.

RESULTS

Fiber size

Extracellular electrical stimulation can excite myelinated axons by generating action potentials at the nodes of Ranvier. For myelinated axons, the activation threshold is largely determined by the spacing between adjacent nodes of Ranvier.[40] This inter-nodal spacing increases as a function of axon diameter and therefore large diameter fibers have a lower threshold than smaller fibers. Previous studies suggest that conventional SCS functions through direct activation of large-diameter myelinated axons within the DC.[14] Therefore, fiber diameter is an important variable to consider because the DC in the human spinal cord consists of axons with a wide range of diameters (average axon diameter ~5.0 μm and a maximum diameter of 16.0 μm at lower thoracic levels).[37] Therefore, we calculated the activation thresholds for axon populations with a range of axon diameters (i.e. 5.7, 7.3, 8.7, 10.0, and 11.5 μm) and densities based on histological data from the human spinal cord (Fig. 4). For these simulations, we used a bipolar stimulation configuration, pulse width of 300 μs, and a pulse frequency of 50 Hz. The results displayed the expected trend of large-diameter fibers having the lowest activation thresholds.

In general, both canonical models exhibited significantly lower activation thresholds relative to the patient-specific model. According to these canonical models, a significant number of small-diameter 5.7 μm axons were activated within the clinically-measured therapeutic range and even below the clinically-measured ST (Fig. 4). The patient-specific model predictions were more representative of the clinical findings and only predicted activation of these smaller diameter fibers at amplitudes above the clinically-measured ST.

Pulse width

For extracellular stimulation, increasing the pulse width leads to an exponential decrease in axonal activation thresholds.[12] Clinical studies have demonstrated that increasing the pulse width can increase total paresthesia coverage, pain relief, and comfort.[23,32] Therefore, we used the patient-specific and canonical models to estimate the ST as a function of pulse width. We defined the model-based ST as the minimum amplitude that produced activation of ≥10% of DC axons.[11] We then compared the model-based ST to the clinically-measured ST (Table 1). Both of the models and the clinical data exhibited an exponential decrease in ST with increasing pulse width (Fig. 5). The clinical ST was 6.6, 3.3, 2.7, 2.5, and 1.9 V for pulse widths of 60, 210, 300, 450, and 1000 μs, respectively. The patient-specific model ST was 7.5, 3.1, 2.6, 2.3, and 2.1 V with a mean absolute percentage error of 8.9% relative to the clinical ST. The canonical model ST was 3.9, 1.6, 1.4, 1.3, and 1.2 V with a mean absolute percentage error of 44.9% relative to the clinical ST. The impedance-matched canonical model ST was 5.8, 2.4, 2.0, 1.7, and 1.6 V with a mean absolute percentage error of 22.0% relative to the clinical ST.

We also calculated the minimum amplitudes required to activate DR fibers as a function of pulse width. In the patient-specific model, DR fiber activation started at 3.0, 1.4, 1.3, 1.2, and 1.1 V for pulse widths of 60, 210, 300, 450, and 1000 μs, respectively. In the canonical model, DR fiber activation started at 2.0, 1.0, 0.93, 0.85, and 0.85 V. In the impedance-matched canonical model, DR fiber activation started at 2.9, 1.4, 1.3, 1.1, and 1.1 V.

Stimulation configuration

During SCS programming procedures, an extensive amount of time is dedicated to finding the combination of cathodes and anodes, also known as the stimulation configuration, that maximizes pain relief and minimizes side effects. Clinicians will select a variety of electrode combinations to "steer" the stimulation to generate an optimal pain-paresthesia overlap. Therefore, we also considered the effects of changing the stimulation configuration on the clinical ST, CT, and DT and on model-predicted activation (Table 1). We tested the following stimulation configurations: bipole, longitudinal tripole, transverse tripole, and pseudo-monopole (Fig. 6). For the tested stimulation configurations, the clinical ST was 2.7, 2.2, 3.3, and 2.9 V, respectively. The patient-specific model ST was 2.6, 2.0, 2.4, and 3.1 V with a mean absolute percentage error of 12.1% relative to the clinical ST. The canonical model ST was 1.4, 1.0, 1.2, and 1.7 V with a mean absolute percentage error of 51.1% relative to the clinical ST. The impedance-matched canonical model ST was 2.0, 1.5, 1.8, and 2.4 V with a mean absolute percentage error of 30.8% relative to the clinical ST.

We also examined the extent of axonal activation predicted by the patient-specific model at the clinical CT and DT. The clinical CT was 4.1, 3.2, 5.0, and 4.3 V. The clinical DT was 5.9,

4.8, 6.4, and 5.8 V. At the clinical CT, the patient-specific model predicted extensive axonal activation within the DC, but activation of only 3.2, 3.1, 3.4, and 3.6% of axons within the dorsal lateral funiculi. At the clinical DT, the patient-specific model predicted considerable activation in the dorsal lateral funiculi of 10.6, 11.8, 7.2, and 11.1% of axons.

Furthermore, we calculated the minimum amplitudes required to activate DR fibers for each stimulation configuration. In the patient-specific model, DR fiber activation started at 1.3, 1.0, 1.3, and 1.2 V for each stimulation configuration. In the canonical model, DR fiber activation started at 0.93, 0.73, 0.93, and 0.95 V. In the impedance-matched canonical model, DR fiber activation started at 1.3, 1.0, 1.3, and 1.2 V.

DISCUSSION

The fundamental goal of this study was to develop a computer model that accounted for 3D patient-specific anatomy and electrode locations to investigate the direct neuromodulatory effects of SCS. To examine the significance of this patient-specific approach, we performed identical simulations with a standard canonical model of SCS. Our results demonstrated considerable differences in axonal activation predicted with the patient-specific model relative to two canonical models. The canonical models predicted markedly lower thresholds for axonal activation (Figs. 4-6). The patient-specific model produced estimates of ST that were closer to the clinical ST measurements (Figs. 5-6). These results suggest that it is beneficial to consider sources of interpatient variability (e.g. anatomy and electrode locations) in computational analysis of SCS.

We also considered the axonal activation predicted at clinical CT and DT. At CT, the patient-specific model predicted extensive activation of DC axons for several different stimulation configurations with little dorsolateral activation. However, at DT, the patient-specific model predicted that activation had spread to the dorsal lateral funiculi. Therefore, axons in the dorsal root entry zone and Lissauer's tract, dorsal spinocerebellar tract, and lateral corticospinal tract may be activated at these stimulation amplitudes, contributing to patient discomfort.

The goal of this type of computational approach is to characterize the direct effects of SCS on different axonal pathways in the spinal cord. Canonical models based on averaged experimental and clinical measurements will continue to be an invaluable tool to improve our scientific understanding of SCS for pain and to improve lead design, stimulation configuration, and waveform parameters.[9,10,12] However, the results of our study suggest that, under various conditions (e.g. patient anatomy, lead placement), patient-specific models may produce predictions of axonal activation within the spinal cord that are more consistent with clinical observations from individual patients. This study also suggests that patient-specific models capture the details necessary to quantitatively describe the axonal response to SCS. Therefore, these patient-specific models could help address scientific questions, such as therapeutic mechanisms of action, related to clinical SCS.

To better understand the mechanisms of action of SCS, it is critical that future research move towards patient-specific approaches to perform systematic studies of SCS in human subjects. One potential approach would be to couple patient-specific computational models with standard clinical outcome measures as well as objective measurements characterizing the physiological effects of SCS (e.g. quantitative sensory testing, functional neuroimaging).[4] This

approach would help explain potential differences in the physiological effects of various SCS paradigms (e.g. tonic, burst, and kilohertz-frequency SCS). By accounting for additional sources of interpatient variability, patient-specific models would further highlight the potential advantages and disadvantages of various lead designs, lead placements, and stimulation configurations. These patient-specific models could also be used to investigate changes in neural activity associated with spinal cord movement (e.g. due to body position, respiration, cough) that are being considered in a novel closed-loop SCS system.[41,42] We believe that this type of patient-specific approach will further elucidate the physiological and technical factors relevant to SCS to improve implementation of current systems as well as innovate novel technologies to significantly improve the clinical outcomes associated with SCS.

Although the results of this study exhibited excellent agreement between the patient-specific model and clinical measurements, this study had several limitations. This study was a proof-of-concept study performed in a single patient. The true validity and utility of this type of approach needs to be validated by extending this approach to multiple patients and testing a wider range of waveform parameters and stimulation configurations. To help make this patient-specific approach feasible, a cohort study would account for multiple sources of interpatient variability and allow for a parameter sensitivity analysis to determine the minimal model complexity necessary to produce accurate model-based predictions. We also assumed that model-based ST corresponded to activation of ≥10% of the DC axons. While this approach has been used in previous SCS modeling studies,[11,15] other modeling studies have suggested that ST corresponds to the activation of only a single large-diameter DC fiber.[14] Therefore, in future studies, it will be critical to examine what degree of model-based activation best correlates with

clinical measurements in a large cohort. Furthermore, we only performed clinical measurements for acute SCS and did not correlate model predictions of axonal activation with clinical outcomes (i.e. pain relief over time). We also tested several sets of stimulation parameters within a single research visit; therefore, it is possible that carryover effects could have influenced the thresholds for individual sets of stimulation parameters. Due to the limited resolution of the clinical MRI scan, we were unable to define patient-specific gray- and white-matter boundaries in the spinal cord and we had to define these boundaries from a cadaver sample[43] that was scaled to match the outer dimensions of the patient's spinal cord. However, it is possible that future improvements in diffusion tensor imaging and fiber tractography could help address this limitation. Another potential limitation was that our axon distributions were based on a study that only considered the superficial (~300 μm) aspect of the DC. Other white matter areas may have different fiber size distributions and therefore different activation thresholds. However, previous studies have shown that the large-diameter myelinated axons in the superficial DC have the lowest thresholds to SCS.[13,14,16] In our models, we represented the electrical properties of the tissue as purely resistive. The capacitive properties of biological tissues could affect the spatiotemporal voltages generated during SCS and the corresponding neural response, especially at higher stimulation frequencies. However, previous studies suggest that tissue capacitance has a negligible filtering effect with conventional SCS parameters, especially during voltage-controlled stimulation.[44–46]

One of the main limitations was estimating DR fiber activation. DR fiber activation can generate uncomfortable paresthesias and/or activation of motor reflex nerves before sufficient activation of DC fibers. One goal of SCS modeling is to guide the selection of stimulation

configurations and waveform parameters that selectively activate DC fibers over DR fibers. In our models, DR fiber activation occurred at amplitudes below the clinical ST. DR thresholds were lowest for fibers that entered the spinal cord near the cathode and the thresholds rapidly increased for fibers a few millimeters above or below the cathode (data not shown). For the bipole configuration, there was also a decrease in activation threshold for DR fibers entering the spinal cord near the anode. We believe that the low thresholds for DR fiber activation were partly attributed to the FEM design. To reduce computational demands, the anatomy of the rootlets is typically not represented in the FEM mesh (Figs. 1 and 3).[14] However, the rootlets have a lower electrical conductivity relative to the surrounding CSF. Therefore, our model, along with the models used in several other studies, may overestimate the excitability of DR fibers for a given fiber size. Future studies should consider explicitly representing the spinal cord rootlets within the FEM.[47] With regards to neural activation at DT, future studies should also consider the range of diameters, number of fibers, as well as functional groups (e.g. proprioceptive, touch) of DR fibers that are activated at stimulation settings that produce unwanted side effects.

To improve the accuracy of the model-based estimations of the voltage distributions generated in the spinal cord, we developed a circuit model of the output of the clinical neurostimulator utilized in this study that we coupled to each FEM (see Supplemental Methods).[36] We used this approach to account for differences in the tissue voltages generated by standard clinical neurostimulators as a function of pulse width and pulse frequency. In the patient-specific and impedance-matched canonical models, we adjusted the electrical conductivity of the encapsulation layer domain so that the model impedances matched the average impedances measured by the clinical programming device. In this study, matching the

model impedance to the clinical impedance was important because the relevant commercial SCS system utilized voltage-controlled stimulation. Electrode impedance variability can produce large differences in the tissue voltages generated during voltage-controlled stimulation.[48] In this study, we only considered a single encapsulation layer domain that would not be able to account for potential electrical heterogeneities in the tissue surrounding individual electrodes. In a previous SCS modeling study, these potential heterogeneities were shown to affect the 3D voltage distributions and corresponding activation within the spinal cord.[29] While our current methodology only permitted us to account for the average electrode impedance, it would be possible to include local encapsulation layer domains at and around each individual electrode.[29] This approach would provide a means to consider electrical heterogeneities and to adjust the model parameters so that each model impedance matched the corresponding clinical impedance for each individual electrode. It should also be noted that while the commercial SCS system considered in this study utilized voltage-controlled stimulation, many SCS systems utilize current-controlled stimulation that would reduce the potential effects of the electrode encapsulation and heterogeneities on the corresponding voltage distributions generated within the spinal cord.[48–50]

CONCLUSION

In this study, we implemented a patient-specific computer modeling approach of SCS. By accounting for patient-specific anatomy, electrode locations, and impedances, theoretical estimates of SCS-induced neuromodulation closely matched the corresponding clinical measurements with far greater accuracy than predictions from a standard canonical model.

These results suggest that patient-specific models can provide quantitative descriptions of the neural response to SCS and serve as a tool to address scientific questions related to clinical SCS as well as inform the development of tools that may guide SCS implantation and programming.

SUPPORTING INFORMATION

Supplemental Methods. The supplemental methods provides additional details with regards to the clinical testing procedures, imaging parameters and segmentation, FEM development and solutions, time-dependent stimulator output, axon models, and overall simulation procedures.

ACKNOWLEDGEMENTS

Scott F. Lempka would like to thank Fang Dong (Cleveland Clinic, Cleveland, OH, USA) for help developing the X-ray computed tomography protocol, Stephen E. Jones (Cleveland Clinic) for assistance with imaging segmentation, and Kabilar Gunalan (Case Western Reserve University, Cleveland, OH, USA) for assistance with computer simulations. Scott F. Lempka would also like to thank Cameron C. McIntyre (Case Western Reserve University) and Vishwanath Sankarasubramanian and Robert Graham (University of Michigan) for helpful comments and discussion.

REFERENCES

1. North RB, Kidd DH, Piantadosi S. Spinal Cord Stimulation Versus Reoperation for Failed

Back Surgery Syndrome: a Prospective, Randomized Study Design. *Acta Neurochir*. 1995;64:106-108.

2. Kemler MA, Barendse GA, van Kleef M, et al. Spinal cord stimulatoin in patients with chronic reflex sympathetic dystrophy. *N Engl J Med*. 2000;343(9):618-624.
3. Kumar K, Taylor RS, Jacques L, et al. The effects of spinal cord stimulation in neuropathic pain are sustained: a 24-month follow-up of the prospective randomized controlled multicenter trial of the effectiveness of spinal cord stimulation. *Neurosurgery*. 2008;63(4):762-770. doi:10.1227/01.NEU.0000325731.46702.D9.
4. Sankarasubramanian V, Harte SE, Chiravuri S, et al. Objective Measures to Characterize the Physiological Effects of Spinal Cord Stimulation in Neuropathic Pain : A Literature Review. *Neuromodulation*. 2018:Epub ahead of print. doi:10.1111/ner.12804.
5. Guan Y, Wacnik PW, Yang F, et al. Spinal Cord Stimulation-induced Analgesia. *Anesthesiology*. 2010;113(6):1392-1405. doi:10.1097/ALN.0b013e3181fcd95c.
6. Song Z, Meyerson BA, Linderoth B. Spinal 5-HT receptors that contribute to the pain-relieving effects of spinal cord stimulation in a rat model of neuropathy. *Pain*. 2011;152(7):1666-1673. doi:10.1016/j.pain.2011.03.012.
7. Zhang TC, Janik JJ, Peters R V., Chen G, Ji R-R, Grill WM. Spinal sensory projection neuron responses to spinal cord stimulation are mediated by circuits beyond gate control. *J Neurophysiol*. 2015;114(1):284-300. doi:10.1152/jn.00147.2015.
8. Youn Y, Smith H, Morris B, Argoff C, Pilitsis JG. The Effect of High-Frequency Stimulation on Sensory Thresholds in Chronic Pain Patients. *Stereotact Funct Neurosurg*. 2015;93(5):355-359. doi:10.1159/000438998.

9. Holsheimer J, Wesselink WA. Effect of Anode-Cathode Configuration on Paresthesia Coverage in Spinal Cord Stimulation. *Neurosurgery*. 1997;41(3):654-660.

10. Struijk JJ, Holsheimer J. Transverse tripolar spinal cord stimulation : theoretical performance of a dual channel system. *Med Biol Eng Comput*. 1996;34(4):273-279.

11. Howell B, Lad SP, Grill WM. Evaluation of intradural stimulation efficiency and selectivity in a computational model of spinal cord stimulation. *PLoS One*. 2014;9(12):e114938. doi:10.1371/journal.pone.0114938.

12. Lee D, Hershey B, Bradley K, Yearwood T. Predicted effects of pulse width programming in spinal cord stimulation: a mathematical modeling study. *Med Biol Eng Comput*. 2011;49(7):765-774. doi:10.1007/s11517-011-0780-9.

13. Lee D, Gillespie E, Bradley K. Dorsal Column Steerability with Dual Parallel Leads using Dedicated Power Sources: A Computational Model. *J Vis Exp*. 2011;(48). doi:10.3791/2443.

14. Holsheimer J. Which neuronal elements are activated directly by spinal cord stimulation. *Neuromodulation*. 2002;5(1):25-31. doi:10.1046/j.1525-1403.2002._2005.x.

15. Capogrosso M, Wenger N, Raspopovic S, et al. A Computational Model for Epidural Electrical Stimulation of Spinal Sensorimotor Circuits. *J Neurosci*. 2013;33(49):19326-19340. doi:10.1523/JNEUROSCI.1688-13.2013.

16. Lempka SF, McIntyre CC, Kilgore KL, Machado AG. Computational Analysis of Kilohertz Frequency Spinal Cord Stimulation for Chronic Pain Management. *Anesthesiology*. 2015;122(6):1362-1376. doi:10.1097/ALN.0000000000000649.

17. Zhang TC, Janik JJ, Grill WM. Modeling effects of spinal cord stimulation on wide-

dynamic range dorsal horn neurons: influence of stimulation frequency and GABAergic inhibition. *J Neurophysiol*. 2014;112(3):552-567. doi:10.1152/jn.00254.2014.

18. Holsheimer J, den Boer JA, Struijk JJ, Rozeboom AR. MR Assessment of the Normal Position of the Spinal Cord in the Spinal Canal. *AJNR Am J Neuroradiol*. 1994;15(5):951-959.
19. Delmotte A, Jacques L, Kumar K, et al. The Franco-Canadian multicolumn spinal cord stimulation prospective study: A subgroup analysis focusing on the decisive role of lead positioning. *Neurochirurgie*. 2015;61(Suppl 1):S83-S89. doi:10.1016/j.neuchi.2014.06.005.
20. Struijk JJ, Holsheimer J, Barolat G, He J, Boom HBK. Paresthesia Thresholds in Spinal Cord Stimulation: A Comparison of Theoretical Results with Clinical Data. 1993;I(2):101-108.
21. Barolat G, Ketcik B, He J. Long-Term Outcome of Spinal Cord Stimulation for Chronic Pain Management. *Neuromodulation*. 1998;1(1):19-29.
22. Aló KM, Redko V, Charnov J. Four Year Follow-up of Dual Electrode Spinal Cord Stimulation for Chronic Pain. *Neuromodulation*. 2002;5(2):79-88.
23. Yearwood TL, Hershey B, Bradley K, Lee D. Pulse Width Programming in Spinal Cord Stimulation: A Clinical Study. *Pain Physician*. 2010;13:321-335.
24. He J, Barolat G, Holsheimer J, Struijk JJ. Perception threshold and electrode position for spinal cord stimulation. *Pain*. 1994;59(1):55-63. doi:10.1016/0304-3959(94)90047-7.
25. Chaturvedi A, Butson CR, Lempka SF, Cooper SE, McIntyre CC. Patient-specific models of deep brain stimulation: Influence of field model complexity on neural activation

predictions. *Brain Stimul*. 2010;3(2):65-77. doi:10.1016/j.brs.2010.01.003.

26. Frankemolle AMM, Wu J, Noecker AM, et al. Reversing cognitive-motor impairments in Parkinson's disease patients using a computational modelling approach to deep brain stimulation programming. *Brain*. 2010;133(3):746-761. doi:10.1093/brain/awp315.
27. Lujan JL, Chaturvedi A, Malone DA, Rezai AR, Machado AG, Mcintyre CC. Axonal pathways linked to therapeutic and nontherapeutic outcomes during psychiatric deep brain stimulation. *Hum Brain Mapp*. 2012;33(4):958-968. doi:10.1002/hbm.21262.
28. McIntyre CC, Chaturvedi A, Shamir RR, Lempka SF. Engineering the next generation of clinical deep brain stimulation technology. *Brain Stimul*. 2015;8(1):21-26. doi:10.1016/j.brs.2014.07.039.
29. Arle JE, Carlson KW, Mei L, Shils JL. Modeling Effects of Scar on Patterns of Dorsal Column Stimulation. *Neuromodulation*. 2014;17(4):320-333. doi:10.1111/ner.12128.
30. Kumar K, Taylor RS, Jacques L, et al. Spinal cord stimulation versus conventional medical management for neuropathic pain: A multicentre randomised controlled trial in patients with failed back surgery syndrome. *Pain*. 2007;132:179-188. doi:10.1016/j.pain.2007.07.028.
31. Struijk JJ, Holsheimer J, K. BHB. Excitation of dorsal root fibers in spinal cord stimulation: A theoretical study. *IEEE Trans Biomed Eng*. 1993;40(7):632-639.
32. Holsheimer J, Buitenweg JR, Das J, De Sutter P, Manola L, Nuttin B. The Effect of Pulse Width and Contact Configuration on Paresthesia Coverage in Spinal Cord Stimulation. *Neurosurgery*. 2011;68(5):1452-1461. doi:10.1227/NEU.0b013e31820b4f47.
33. Sankarasubramanian V, Buitenweg JR, Holsheimer J, Veltink PH. Staggered Transverse

Tripoles With Quadripolar Lateral Anodes Using Percutaneous and Surgical Leads in Spinal Cord Stimulation. *Neurosurgery*. 2013;72(3):483-491. doi:10.1227/NEU.0b013e31827d0e12.

34. Ladenbauer J, Minassian K, Hofstoetter US, Dimitrijevic MR, Ratty F. Stimulation of the Human Lumbar Spinal Cord With Implanted and Surface Electrodes - A Computer Simulation Study. *IEEE Trans Neural Syst Rehabil Eng*. 2010;18(6):637-645.
35. Gunalan K, Chaturvedi A, Howell B, et al. Creating and parameterizing patient-specific deep brain stimulation pathway-activation models using the hyperdirect pathway as an example. *PLoS One*. 2017;12(4):e0176132.
36. Lempka SF, Howell B, Gunalan K, Machado AG, McIntyre CC. Characterization of the stimulus waveforms generated by implantable pulse generators for deep brain stimulation. *Clin Neurophysiol*. 2018;129(4):731-742. doi:10.1016/j.clinph.2018.01.015.
37. Feirabend HKP, Choufoer H, Ploeger S, Holsheimer J, van Gool JD. Morphometry of human superficial dorsal and dorsolateral column fibres: significance to spinal cord stimulation. *Brain*. 2002;125:1137-1149.
38. McIntyre CC, Richardson AG, Grill WM. Modeling the Excitability of Mammalian Nerve Fibers: Influence of Afterpotentials on the Recovery Cycle. *J Neurophysiol*. 2002;87:995-1006.
39. Struijk JJ, Holsheimer J, Boom HBK. Excitation of Dorsal Root Fibers in Spinal Cord Stimulation - A Theoretical Study. *IEEE Trans Biomed Eng*. 1993;40(7):632-639.
40. Rattay F. High frequency electrostimulation of excitable cells. *J Theor Biol*. 1986;123:45-54. doi:10.1016/S0022-5193(86)80234-X.

41. Parker JL, Karantonis DM, Single PS, Obradovic M, Cousins MJ. Compound action potentials recorded in the human spinal cord during neurostimulation for pain relief. *Pain*. 2012;153(3):593-601. doi:10.1016/j.pain.2011.11.023.

42. Russo M, Cousins MJ, Brooker C, et al. Effective Relief of Pain and Associated Symptoms With Closed-Loop Spinal Cord Stimulation System: Preliminary Results of the Avalon Study. *Neuromodulation*. 2018;21(1):38-47. doi:10.1111/ner.12684.

43. Kameyama T, Hashizume Y, Sobue G. Morphologic Features of the Normal Human Cadaveric Spinal Cord. *Spine (Phila Pa 1976)*. 1996;21(11):1285-1290.

44. Plonsey R, Heppner DB. Considerations of quasi-stationarity in electrophysiological systems. *Bull Math Biophys*. 1967;29(4):657-664. doi:10.1007/BF02476917.

45. Butson CR, McIntyre CC. Tissue and electrode capacitance reduce neural activation volumes during deep brain stimulation. *Clin Neurophysiol*. 2005;116(10):2490-2500. doi:10.1016/j.clinph.2005.06.023.

46. Bossetti CA, Birdno MJ, Grill WM. Analysis of the quasi-static approximation for calculating potentials generated by neural stimulation. *J Neural Eng*. 2008;5(1):44-53. doi:10.1088/1741-2560/5/1/005.

47. Wagner FB, Mignardot J, Goff-mignardot CG Le, et al. Targeted neurotechnology restores walking in humans with spinal cord injury. *Nature*. 2018. doi:10.1038/s41586-018-0649-2.

48. Lempka SF, Johnson MD, Miocinovic S, Vitek JL, Mcintyre CC. Current-controlled deep brain stimulation reduces in vivo voltage fluctuations observed during voltage-controlled stimulation. *Clin Neurophysiol*. 2010;121(12):2128-2133.

doi:10.1016/j.clinph.2010.04.026.

49. Miocinovic S, Lempka SF, Russo GS, et al. Experimental and theoretical characterization of the voltage distribution generated by deep brain stimulation. *Exp Neurol*. 2009;216:166-176. doi:10.1016/j.expneurol.2008.11.024.

50. Lempka SF, Patil PG. Innovations in spinal cord stimulation for pain. *Curr Opin Biomed Eng*. 2018;8:51-60. doi:10.1016/j.cobme.2018.10.005.

Figure Legends

Figure 1. Patient-specific finite element model (FEM). a. We used preoperative MRI scans to define the participant's anatomy (e.g. spinal cord, cerebrospinal fluid (CSF), spine) and a postoperative X-ray computed tomography (CT) scan to define the 3D electrode locations. b. We coregistered the 3D objects segmented from the preoperative and postoperative images to define a patient-specific FEM. The figure on the top right shows outlines of the 3D FEM objects in the preoperative MRI. The figure on the bottom right shows the voltages generated on the surface of the spinal cord for a -1 V bipolar stimulus (Note: In this figure, the electrode array and spinal cord are not drawn on the same scale).

Figure 2. Axon models. a. In our analysis, we included multi-compartment cable models of myelinated axons[38] running through the white matter of the spinal cord. We also included dorsal root (DR) fibers that consisted of a mother fiber and a bifurcated daughter fiber running along the dorsal columns. b. We generated axon populations that covered a range of diameters (i.e. 5.7-11.5 μm) to match the axon diameters and densities measured in the human spinal cord.[37] For computational simplicity, we only used 1% of the true anatomical densities. (Note: In this figure, the axon diameters are not drawn to scale).

Figure 3. Axonal response to spinal cord stimulation (SCS). a. Axial and sagittal views of isopotential lines of the extracellular voltages generated by SCS. The voltage distributions were calculated from the patient-specific finite element model. b. To estimate the direct axonal response to SCS, we interpolated the SCS-induced extracellular voltages onto the axon models.

With sufficient depolarization, action potentials were initiated in an axon and propagated in both orthodromic and antidromic directions. The figure shows the time-dependent transmembrane voltages at several nodes in a dorsal column (DC) axon and illustrates action potential generation with a 50 Hz SCS waveform.

Figure 4. SCS activation thresholds as a function of axon diameter. a. Thresholds for individual axons within the dorsal columns (DC) as a function of axon diameter. We performed simulations for the patient-specific and both canonical models. The clinical sensory threshold (ST) and discomfort threshold (DT) are indicated by the black horizontal lines. b. Model axons activated at the clinical ST as a function of axon diameter. The top, middle, and bottom rows show axial cross sections of the spinal cord for the patient-specific, canonical, and impedance-matched canonical models, respectively. Activated axons are shown in red, green, and blue for the patient-specific, canonical, and impedance-matched canonical models, respectively. We calculated thresholds for a bipolar stimulation with a pulse width of 300 μs and a pulse frequency of 50 Hz.

Figure 5. Sensory threshold (ST) as a function of pulse width. We measured the clinical ST as a function of pulse width. We also estimated the model ST (i.e. minimum pulse amplitude to activate ≥10% of the dorsal column axons) for the patient-specific and both canonical models. We calculated the ST for bipolar stimulation with a pulse frequency of 50 Hz.

Figure 6. Sensory threshold (ST) for various stimulation configurations. We measured the clinical ST and calculated the model ST (i.e. minimum pulse amplitude to activate ≥10% of the dorsal column axons) for the patient-specific and both canonical models. We determined the ST for the following stimulation configurations: bipole (1st column), longitudinal guarded cathode (2nd column), transverse guarded cathode (3rd column), and pseudo-monopole (4th column). We determined the ST for a pulse width of 300 μs and a pulse frequency of 50 Hz.

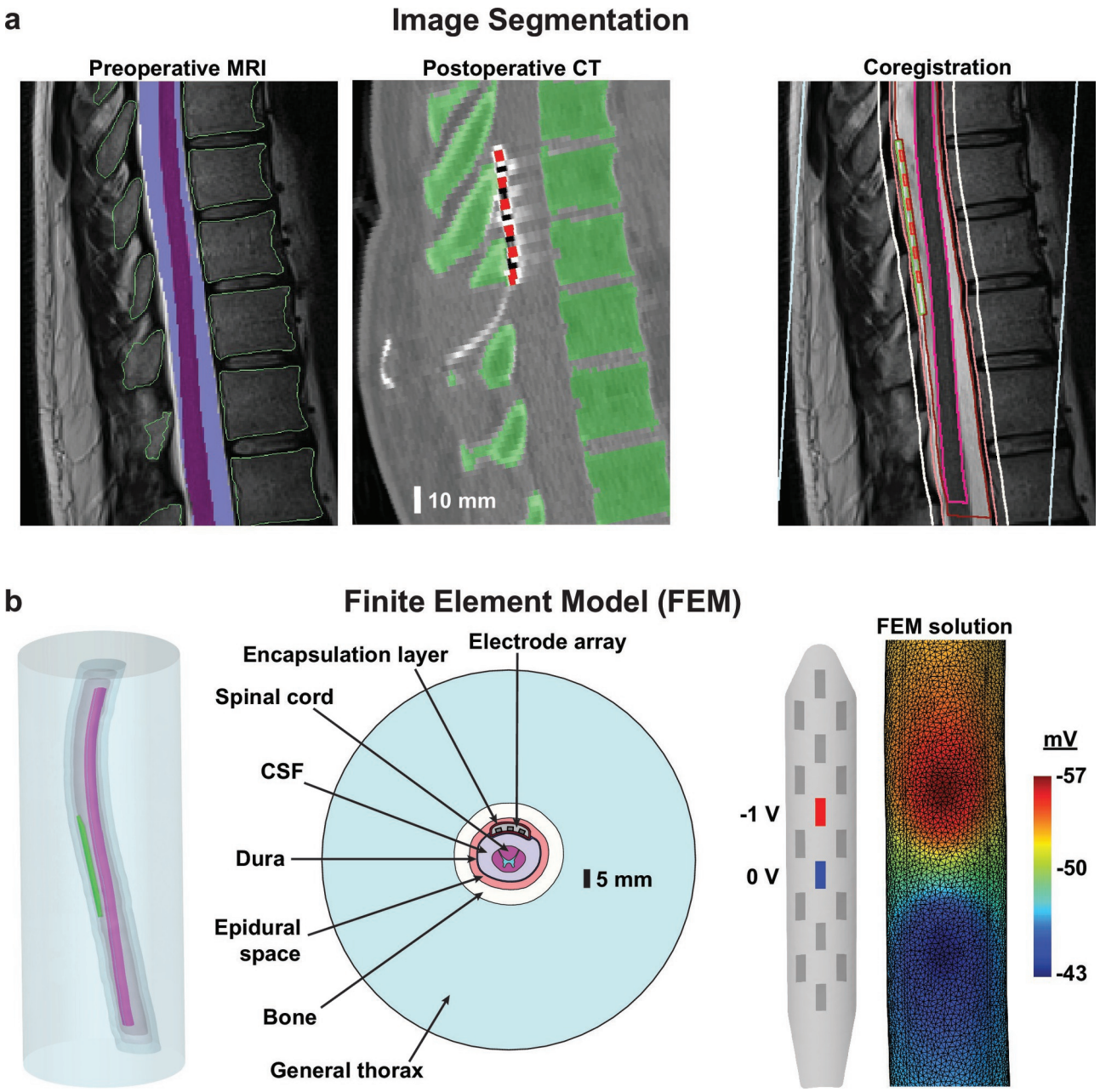

ner_13037_figure 1-r1-01.eps

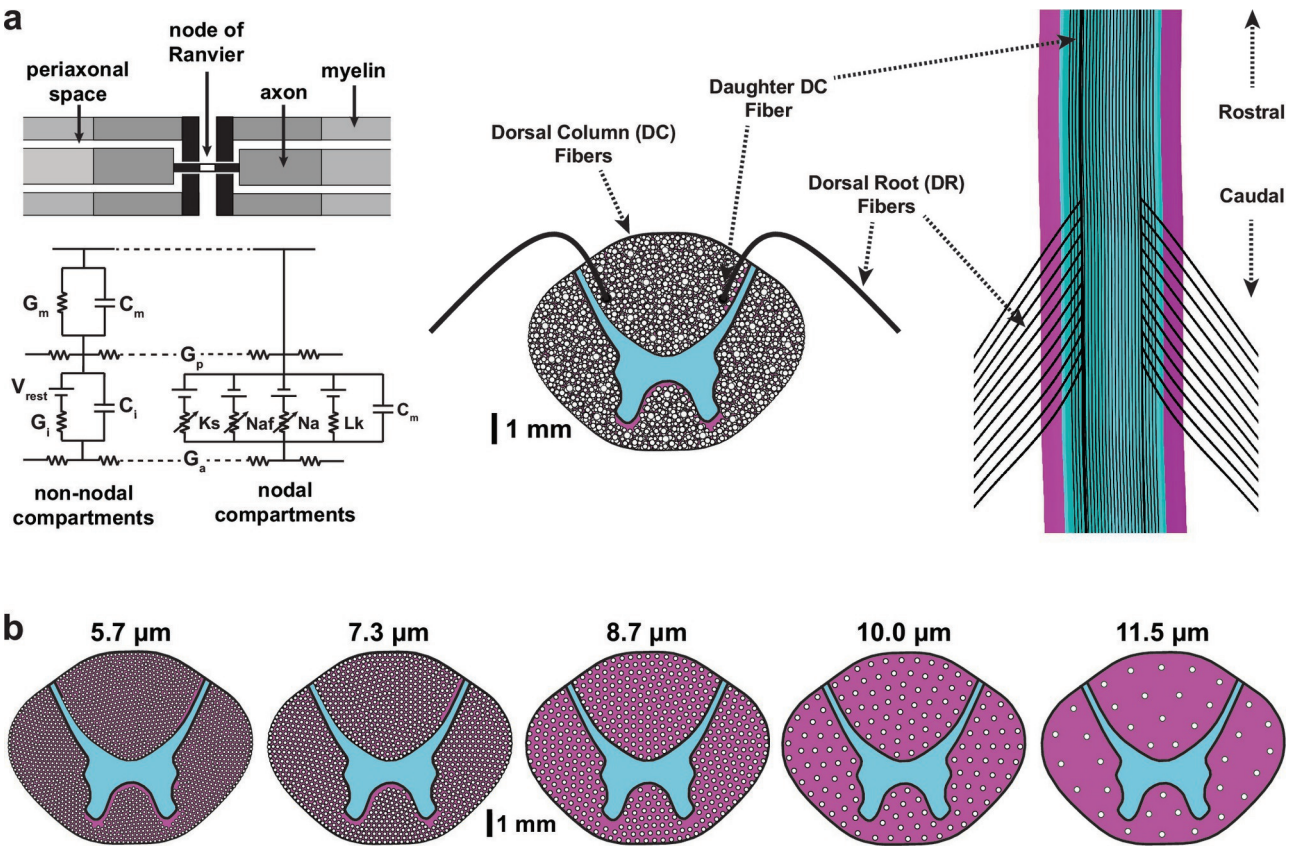

ner_13037_figure 2-r1-01.eps

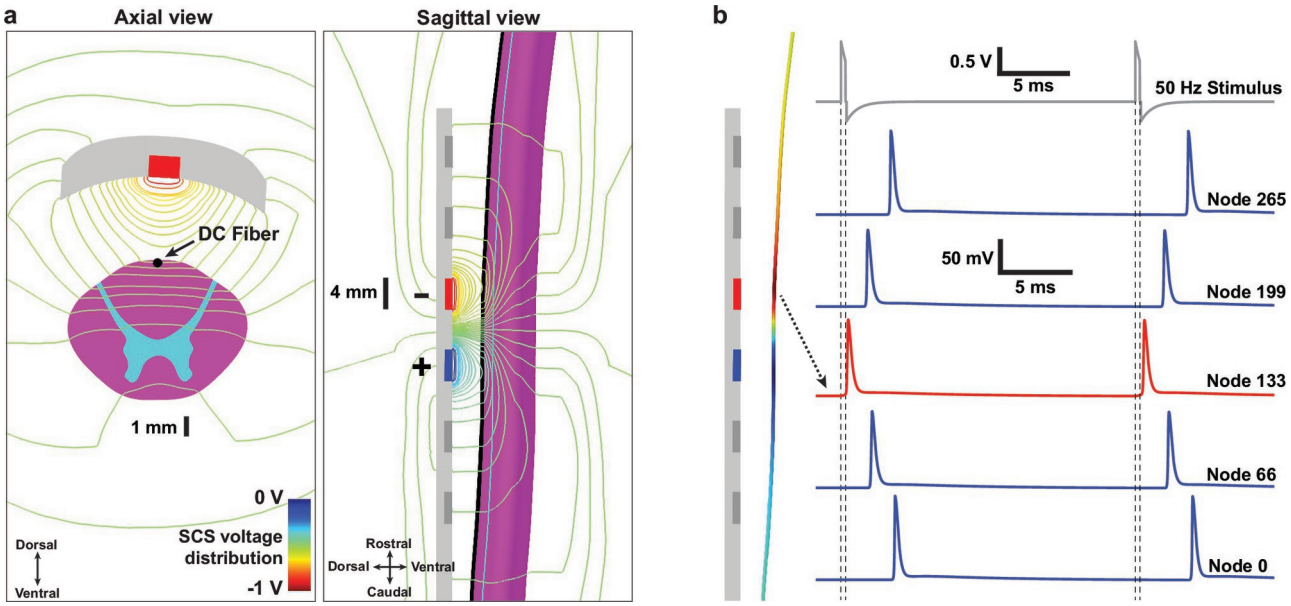

ner_13037_figure 3-r1-01.eps

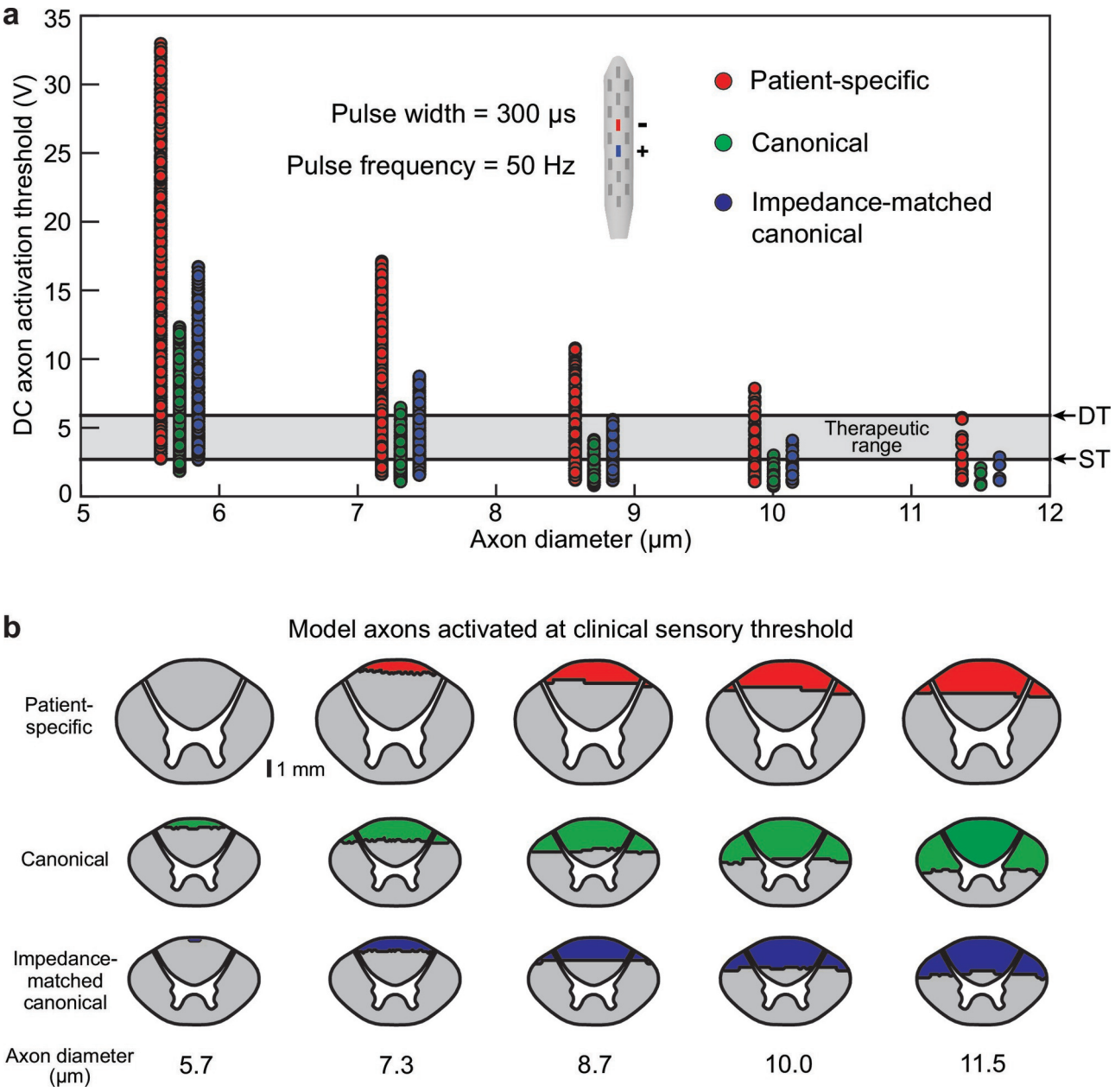

ner_13037_figure 4-r1-01.eps

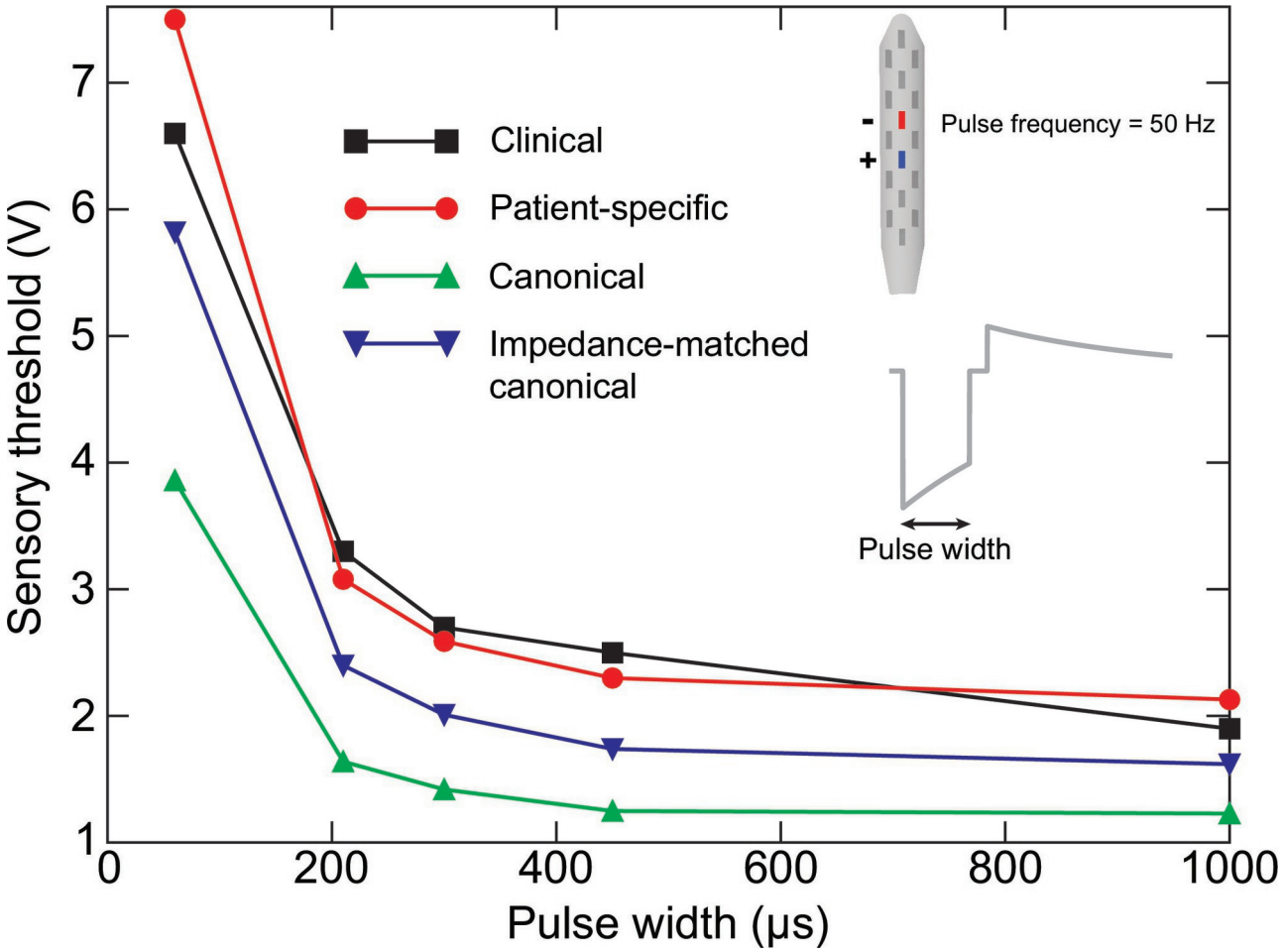

ner_13037_figure 5-r1-01.eps

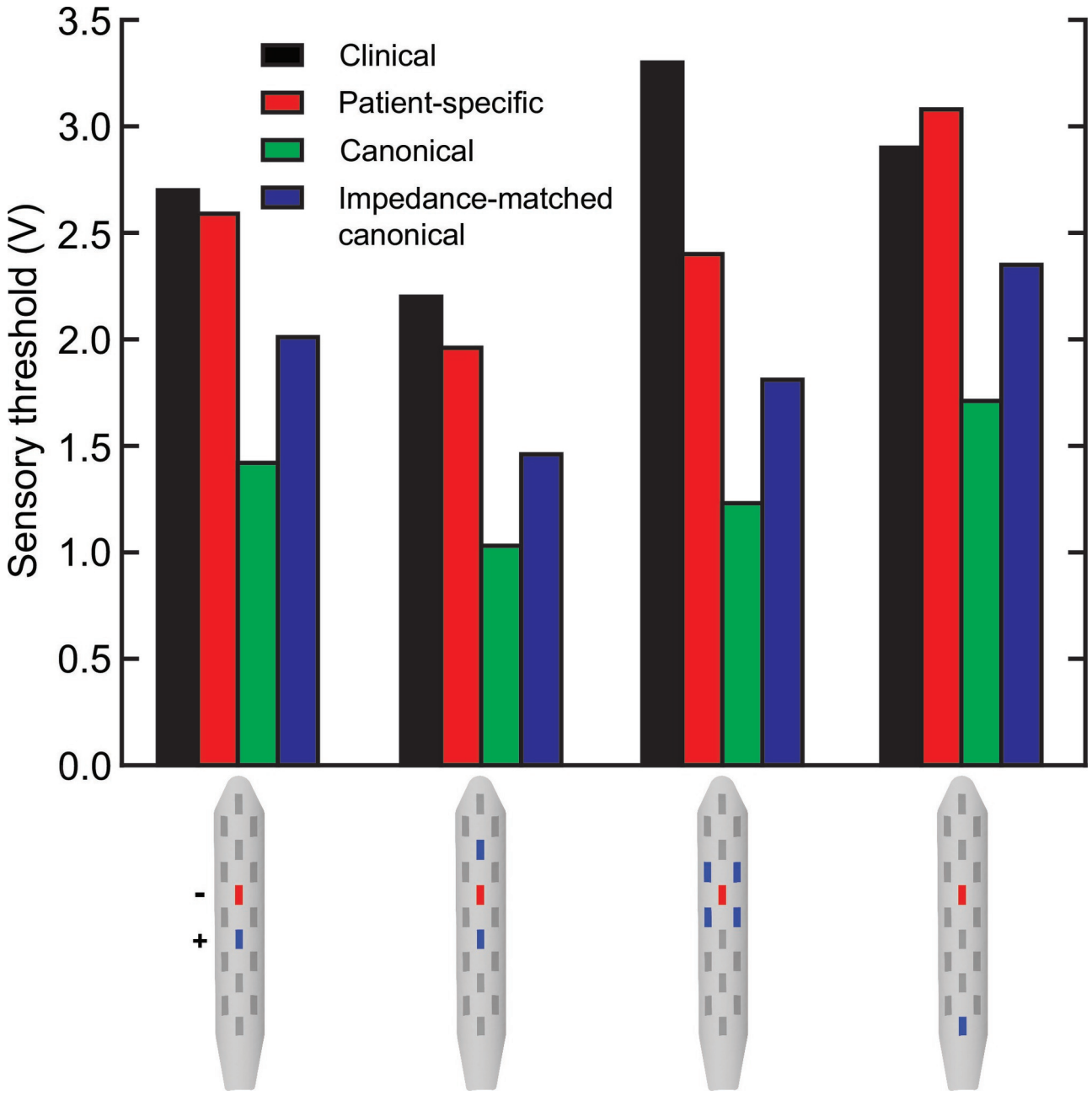

ner_13037_figure 6-r1-01.eps

Blackwell Publishing

Neuromodulation: Copyright Assignment Form

Author's name: ...Scott F. Lempka, PhD.....

Author's address: ...2800 Plymouth Road, NCRC 14-184, Ann Arbor, MI 48109-2800.....

.....

Title of article ("Article"): ...Patient-specific analysis of neural activation during spinal cord stimulation for pain.....
.....

.....

Manuscript no. (if known): .....

Names of all authors in the order in which they appear in the Article: ...Scott F. Lempka, Hans Zander, Carlos J. Anaya, Alexandria Wyant, John G. Ozinga, IV, Andre G. Machado.....

To enable Wiley-Blackwell to publish your Article in Neuromodulation (the Journal), the ownership of copyright must be established. The Article is deemed to include all material submitted for publication with the exception of Letters, and includes the text, figures, tables, author contact details and all supplementary material accompanying the Article.

Please read this form carefully, sign at the bottom (if your employer owns copyright in your work, arrange for your employer to sign where marked), and return the ORIGINAL to the address below as quickly as possible. (US Federal Government authors please note: your Article is in the public domain.)

Your Article will not be published unless a Copyright Assignment Form has been signed and received by Wiley-Blackwell.

Please note: You retain the following rights to re-use the Article, as long as you do not sell or reproduce the Article or any part of it for commercial purposes (i.e. for monetary gain on your own account or on that of a third party, or for indirect financial gain by a commercial entity). These rights apply without needing to seek permission from Wiley-Blackwell.

- **Prior to acceptance:** We ask that as part of the publishing process you acknowledge that the Article has been submitted to the Journal. You will not prejudice acceptance if you use the unpublished Article, in form and content as submitted for publication in the Journal, in the following ways:
  - sharing print or electronic copies of the Article with colleagues;
  - posting an electronic version of the Article on your own personal website, on your employer's website/repository and on free public servers in your subject area.
- **After acceptance:** Provided that you give appropriate acknowledgement to the Journal, International Neuromodulation Society and Wiley-Blackwell, and full bibliographic reference for the Article when it is published, you may use the accepted version of the Article as originally submitted for publication in the Journal, and updated to include any amendments made after peer review, in the following ways:
  - you may share print or electronic copies of the Article with colleagues;
  - you may use all or part of the Article and abstract, without revision or modification, in personal compilations or other publications of your own work;
  - you may use the Article within your employer's institution or company for educational or research purposes, including use in course packs;
  - 12 months you may post an electronic version of the Article on your own personal website, on your employer's website/repository and on free public servers in your subject area. Electronic versions of the accepted Article must include a link to the published version of the Article together with the following text: 'The definitive version is available at www.neuromodulationjournal.com.

Please note that you are not permitted to post the Wiley-Blackwell PDF version of the Article online.

All requests by third parties to re-use the Article in whole or in part will be handled by Wiley-Blackwell. Any permission fees will be retained by the Journal. All requests to adapt substantial parts of the Article in another publication (including publication by Wiley-Blackwell) will be subject to your approval (which is deemed to be given if we have not heard from you within 4 weeks of your approval being sought by us writing to you at your last notified address). Please address any queries to journalsrights@oxon.blackwellpublishing.com.

In signing this Agreement:

1. You hereby warrant that this Article is an original work, has not been published before and is not being considered for publication elsewhere in its final form either in printed or electronic form;
2. You hereby warrant that you have obtained permission from the copyright holder to reproduce in the Article (in all media including print and electronic form) material not owned by you, and that you have acknowledged the source;
3. You hereby warrant that this Article contains no violation of any existing copyright or other third party right or any material of an obscene, indecent, libellous or otherwise unlawful nature and that to the best of your knowledge this Article does not infringe the rights of others;
4. You hereby warrant that in the case of a joint Article you have obtained, in writing, authorization to enter into this Agreement on their behalf and that all co-authors have read and agreed the terms of this Agreement;

6. You will indemnify and keep indemnified the Editors/International Neuromodulation Society and Wiley-Blackwell against all claims and expenses (including legal costs and expenses) arising from any breach of this warranty and the other warranties on your behalf in this Agreement.

By signing this Agreement you agree that Wiley-Blackwell may arrange for the Article to be:

- Published in the above Journal, and sold or distributed, on its own, or with other related material;
- Published in multi-contributor book form or other edited compilations by Wiley-Blackwell;
- Reproduced and/or distributed (including the abstract) throughout the world in printed, electronic or any other medium whether now known or hereafter devised, in all languages, and to authorize third parties (including Reproduction Rights Organizations) to do the same;
- You agree to Wiley-Blackwell using any images from the Article on the cover of the Journal, and in any marketing material.

You authorize Wiley-Blackwell to act on your behalf to defend the copyright in the Article if anyone should infringe it, although there is no obligation on Wiley-Blackwell to act in this way.

Wiley-Blackwell undertakes that every copy of the Article published by Wiley-Blackwell will include the full bibliographic reference for your Article, together with the copyright statement.

☒ **BOX A: to be completed if copyright belongs to you**
You hereby assign to Wiley-Blackwell/Society copyright in the Article including the abstract for the full period of copyright and all renewals, extensions, revisions and revivals throughout the world in any form and in all languages. Wiley-Blackwell may assign the rights granted in this Copyright Assignment Form.

☐ **BOX B: to be completed if copyright belongs to your employer (e.g. HMSO, CSIRO)**
The copyright holder grants Wiley-Blackwell/Society an exclusive licence to publish the Article including the abstract in printed and electronic form, in all languages, and to administer subsidiary rights agreements with third parties for the full period of copyright and all renewals, extensions, revisions and revivals.

Print Name of Copyright holder: .....
This will be printed on the copyright line on each page of the Article. It is your responsibility to provide the correct information of the copyright holder.

☐ **BOX C: to be completed if the Article is in the public domain (e.g. US Federal Government employees)** You certify that the Article is in the public domain. No licence to publish is therefore necessary.

Signature (on behalf of all co-authors (if any)) **Print name: ...Scott Lempka, PhD.....**

Scott Lempka
..... **Date: .....08/13/2018.....**

If your employer claims copyright in your work, this form must also be signed below by a person authorized to sign for and on behalf of your employer, as confirmation that your employer accepts the terms of this licence.

Signature (on behalf of the employer of the author (s)) **Print name:.....**

Print name of employer: .....

..... **Date: .....**

The rights conveyed in this assignment will only apply upon acceptance of your Article for publication.

We may in the future send you information on relevant Blackwell publications by mail or email. If you do not wish to receive these mailings please check the box(es) ❑ mail ❑ email.

Please return the signed form to:
Tia Sofatzis
Managing Editor
Neuromodulation, Journal of the INS
2000 Van Ness Avenue, Suite 402
San Francisco, CA 94109
USA
Or by email to: tsofatzis@neuromodulation.com

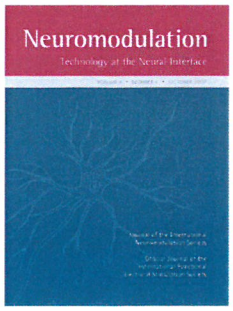

Statement on Real or Perceived Conflicts of Interest for Authors

Information pertaining to *all* authors must be entered on this form

Neuromodulation: Technology at the Neural Interface has a primary responsibility to its readers and to the public to provide in its pages clear and unbiased scientific results and analyses. Although we rely on the expertise of our Editors, Editorial Board members and our peer reviewers to help us accomplish this, we believe that our readers should be informed of additional relationships of our authors that could pose a conflict of interest. Thus, for readers to evaluate the data and opinions presented in *Neuromodulation: Technology at the Neural Interface*, they must be informed of financial and other interests of our authors that may be at odds with unbiased presentation of data or analysis.

In compliance with the International Committee of Medical Journal Editors' (ICMJE) Uniform Requirements for Manuscripts Submitted to Biomedical Publications.[1] (http://www.icmje.org/) *Neuromodulation* requires that all manuscripts should be accompanied by clear disclosures from all authors of their affiliations, funding sources, or financial holdings that might raise questions about possible sources of bias. Disclosure is accomplished in three ways:

First, by a complete listing of the current institutional affiliations of the authors.
This list must include academic as well as corporate and other industrial affiliations. As the editors deem appropriate, items in this list will be included in the author affiliations printed in the manuscript. Please indicate below:

- [X] All affiliations of all authors are listed on the title page of the paper.
- [ ] Additional affiliations not on the title page are:

Second, through the acknowledgment of all financial contributions to the work being reported, including contributions "in kind."
All funding sources will be listed in the published manuscript. Please indicate below:

- [X] All funding sources for this study are listed in the acknowledgement section of the paper.
- [ ] Additional funding sources not noted in the manuscript are:

Reference
1. International Committee of Medical Journal Editors. Uniform requirements for manuscripts submitted to biomedical journals. http://www.icmje.org.

Third, through the execution of a statement disclosing to the Editors all financial holdings, professional affiliations, advisory positions, board memberships, patent holdings and the like that might bear a relationship to the subject matter of the contribution.
The Editors will determine whether the material disclosed to them should be published as part of the article**.** Please check the appropriate items below:

The following are declarable relationships:

Financial: Significant financial interest (equity holdings or stock options) in any corporate entity dealing with the material or the subject matter of this contribution. Please disclose the entity and the nature of the holding.

☐ None
☒ One or more authors has a financial relationship, as described below:

SFL holds stock options in Presidio Medical, Inc. AGM has distribution rights to Cardionomic, Inc. and Enspire DBS, Inc.

Management/Advisory Affiliations: Within the last 3 years, status as an officer, a member of the Board, or a member of an Advisory Committee of any entity engaged in activity related to the subject matter of this contribution. Please disclose the nature of these relationships and the financial arrangements.

☐ None
☒ One or more authors has a management/advisory relationship, as described below:

SFL serves on the scientific advisory board for Presidio Medical, Inc.

Paid Consulting: Within the last 3 years, receipt of consulting fees, honoraria, speaking fees, travel fees or expert testimony fees from entities that have a financial interest in the results and materials of this study. Please enumerate.

☐ None
☒ One or more authors has a paid consulting relationship, as described below:

AGM is a paid consultant of St. Jude Medical.

Patents: A planned, pending, or awarded patent on this work by any of the authors or their institutions. Please explain.

☐ None
☒ One or more authors or the authors' institutions has a patent related to this work, as described below:

The Cleveland Clinic holds patents related to spinal cord stimulation with SFL and AGM as inventors. Case Western Reserve University holds a patent related to neurostimulation for pain with SFL as one of the inventors.

☒ **All authors declare that we have read *Neuromodulation: Technology at the Neural Interface's* full Conflict of Interest Policy and have disclosed all declarable relationships as defined therein, if any.**

Manuscript Number_____

Title: Patient-specific analysis of neural activation during spinal cord stimulation for pain

First Author: Scott F. Lempka, PhD

Signature: 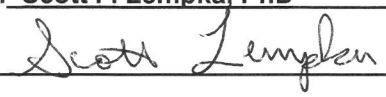 **Date:** 08/13/2018

This form must be completed and submitted to the **Neuromodulation Editorial Office** prior to your manuscript's publication. Submit form to:

Neuromodulation, 2000 Van Ness Avenue, Suite 402, San Francisco, CA 94109 USA

Fax: +1.415.683.3218 Email: INS@neuromodulation.com

Neuromodulation: Technology at the Neural Interface

Authorship and Contributorship Guidelines

Neuromodulation: Technology at the Neural Interface bases its authorship criteria on those outlined by the International Committee of Medical Journal Editors' (ICMJE) Uniform Requirements for Manuscripts Submitted to Biomedical Publications. (http://www.icmje.org/ethical_1author.html) [1] The corresponding author must submit the manuscript, related files, and all required data and information. From the point of submission until publication, all communication related to the manuscript will be directed to and received from the designated corresponding author only.

Authorship credit should be based on:

1) substantial contribution to conception and design, or acquisition of data, or analysis and interpretation of data;

2) drafting the article or reviewing it critically for important intellectual content; and

3) final approval of the version to be published.

Authors should meet conditions 1, 2, and 3. [1]

When a large, multi-center group has conducted the work, the group should identify the individuals who accept direct responsibility for the manuscript. These individuals should fully meet the criteria for authorship defined above and editors will ask these individuals to complete Neuromodulation Authorship and Conflict of Interest forms. When submitting a group author manuscript, the corresponding author should clearly indicate the preferred citation and should clearly identify all individual authors as well as the group name.

Acquisition of funding, collection of data, or general supervision of the research group, alone, does not justify authorship. All persons designated as authors should qualify for authorship, and all those who qualify should be listed. Each author should have participated sufficiently in the work to take public responsibility for appropriate portions of the content.

Authors are required to:

1) confirm that all authors meet the criteria for authorship stated in the Uniform Requirements for Manuscripts Submitted to Biomedical Journals;
2) confirm that everyone who contributed significantly to the work and has approved the submitted manuscript;
3) declare whether the authors had assistance with study design, data collection, data analysis, or manuscript preparation and disclose the source of any material or financial support;
4) verify the accuracy of the content and confirm that the content of the manuscript represents their work/opinions and not those of the sponsoring agent(s), if any.

Within the "Acknowledgment" section and under the subheading 'Author Contributions,' all authors' specific areas of contributions should be listed. In addition, any writer or editor assisting the authors, who does not fulfill all criteria for authorship, should be acknowledged here, including a description of his or her role in the submission, affiliation(s), and source(s) of support. Examples of those who might be acknowledged include a person who provided technical help, editing assistance, writing assistance (i.e. a ghost writer), or a department chair who provided only general support. If such assistance was available, the authors should disclose the identity of the individuals who provided this assistance and the entity that supported it. Financial and material support should also be acknowledged.

Reference

1. International Committee of Medical Journal Editors. Uniform requirements for manuscripts submitted to biomedical journals. http://www.icmje.org.

Neuromodulation Authorship and Contributorship Form

Manuscript Title: Patient-specific analysis of neural activation during spinal cord stimulation for pain

1) Please confirm the following:

☒ **Confirm the accuracy of the content and that the content of the manuscript represents the authors' work/opinions and not those of the sponsoring agent(s), if any.**

☒ **Confirm that the corresponding author agrees to communicate with all other authors and will obtain their approval for the final version to be published.**

☒ **Confirm that all authors are listed and have made substantial contributions to:**
- the research design, or the acquisition, analysis or interpretation of data; and to
- drafting the paper or reviewing it critically;
- and that all authors have approved the submitted version

2) Give a short description of each individual's contribution to the research and its publication (e.g. designed study, analyzed data, drafted paper).

Sample authorship description and acknowledgement:
Drs. A, B and C designed and conducted the study, including patient recruitment, data collection, and data analysis. Dr. A prepared the manuscript draft with important intellectual input from Drs. B and C. All authors approved the final manuscript. [Insert name of organization] provided funding for the study, statistical support in analyzing the data with input from Drs. A, B and C, and also provided funding for editorial support. Drs. A, B and C had complete access to the study data. We would like to thank Dr. D for her editorial support during preparation of this manuscript

---

All authors were responsible for the study concept and design. SFL and JGO performed the data acquisition. SFL, HZ, CJA performed the model design. SFL performed the model analysis. SFL prepared the manuscript draft, figures, and table with guidance from AW, JGO, and AGM. All authors provided intellectual input and assisted with manuscript revisions. All authors approved the final version of the manuscript.

3) Was this research or its publication assisted by any non-financial or 'in-kind' contributions? (e.g. provision of study design, data collection, data analysis, writing assistance, literature searching, administrative support, supply of materials).

☐ **YES** ☒ **NO**

If yes, state the identity of the individuals who provided this assistance and disclose the source of any material or financial support:

Corresponding Author: Scott Lempka **Date:** 08/13/18

SUPPLEMENTAL METHODS

Clinical testing

At the time of the research visit, the participant was using four stimulation programs to help manage his chronic pain. We asked the participant which individual program provided the most significant pain relief. This program utilized contact 7 (C7) as the cathode (Fig. S1). Therefore, we used C7 as the cathode in our study.

We measured the sensory threshold, comfort threshold, and discomfort threshold for several sets of stimulation parameters. We varied the pulse width and the stimulation configuration. For each set of stimulation parameters, we used a pulse frequency of 50 Hz. When varying the pulse width, we used C7 as the cathode and C8 as the anode. When varying the stimulation configuration, we used a pulse width of 300 μs and tested the following stimulation configurations ((-) = cathode; (+) = anode): bipole = C7(-),C8(+); longitudinal guarded cathode = C6(+),C7(-),C8(+); transverse guarded cathode = C1(+),C2(+),C7(-),C12(+),C13(+); and pseudo-monopole = C7(-),C10(+) (Fig. S1). We used the hand-held N'Vision Clinician Programmer Model 8840 (Medtronic, Inc., Minneapolis, MN, USA) to adjust the stimulation parameters. All stimulation parameters were tested in a randomized order.

Because the participant's commercial SCS system utilized voltage-controlled stimulation, it was important to consider the effects of electrode impedance on stimulation thresholds. Therefore, we measured the bipolar electrode impedances relative to C0 for each of the remaining 15 electrodes at the end of the research testing using the built-in functionality of the implantable (IPG) and the N'Vision Clinician Programmer.

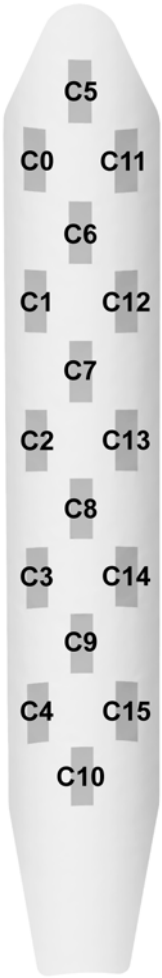

Figure S1. Individual electrode numbers for the SCS array (e.g. C0 = contact 0).

Imaging parameters

Magnetic resonance imaging (MRI) parameters. We used preoperative MRI scans without contrast of the thoracic spine to define the patient-specific anatomy. These images were obtained as part of the participant's standard clinical care for SCS. These scans consisted of T2-weighted images in the sagittal and axial orientations as well as T1-weighted images with a sagittal orientation. The sagittal T2-weighted images were obtained with the following imaging parameters: scanning sequence = spin echo, magnetic field = 1.5 T, pixel spacing = 0.725 mm, field of view = 325 mm, number of slices = 17, slice increment = 3.60 mm, slice thickness = 3.00 mm. The axial T2-weighted images were obtained with the following imaging parameters:

scanning sequence = gradient echo, magnetic field = 1.5 T, pixel spacing = 0.391 mm, field of view = 200 mm, number of slices = 42, slice increment = 5.20 mm, slice thickness = 4.00 mm. The sagittal T1-weighted images were obtained with the following imaging parameters: scanning sequence = spin echo, magnetic field = 1.5 T, pixel spacing = 0.725 mm, field of view = 325 mm, number of slices = 19, slice increment = 3.30 mm, slice thickness = 3.00 mm.

Computed tomography (CT) parameters. We used a modified research CT protocol to image the lower thoracic spine and the implanted SCS electrodes. The CT scan was obtained with the following acquisition parameters: peak voltage = 120 kV, X-ray tube current = 135 mA, collimation = 0.6 mm, field of view = 164 mm, pixel size = 0.320 mm. The CT scans had the following reconstruction parameters: kernel value = B40s, extended CT scale, axial slice thickness = 0.75 mm (number of slices = 302) and 2.00 mm (number of slices = 114).

Image segmentation

We used preoperative MRI images to segment relevant components of the participant's anatomy. We used a combination of T1-weighted and T2-weighted images to segment the participant's spinal cord, cerebrospinal fluid (CSF), epidural fat, and spine. We used the postoperative CT scan to determine the location of the individual SCS electrodes and segment the participant's spine. All image segmentations were manually performed and converted to 3D surface objects in the Mimics Innovation Suite (Materialise, Leuven, Belgium).

To coregister the 3D objects from the preoperative MRI data and the postoperative CT data, we first imported the 3D objects into the 3-matic module within the Mimics Innovation Suite. We performed this coregistration process in two steps using the spine segmentations from both the MRI and CT datasets. The first step was to use the 'N points registration' function in 3-matic to coregister the spine by manually selecting matching anatomical landmarks on the preoperative and postoperative spines (e.g. points near the midline at the top and bottom of the vertebral bodies, dorsal ends of the vertebral processes). This step moved the 3D spine object

segmented from the postoperative CT image along with the electrode segmentations to the same coordinate system as the preoperative MRI. In the second step, we refined this coregistration with the 'Global registration' function in 3-matic.

Patient-specific finite element model

In the 3-matic module, we then used the coregistered 3D surface objects of the patient-specific anatomy and electrode locations to define a patient-specific finite element model (FEM) (Fig. S2a). To define the spinal cord, we determined the boundaries between the gray and white matter from a human cadaver sample of the lower thoracic spinal cord.[1] We then scaled the anteroposterior and mediolateral dimensions of this spinal cord cross section to match the average measurements of the participant's spinal cord anatomy at the T9 spinal level (i.e. anteroposterior = 7 mm and mediolateral = 9 mm). To create a 3D spinal cord containing gray and white matter domains, we then swept this 2D spinal cord cross section along the trajectory of the participant's spinal cord as determined by the preoperative MRI. We used the CSF surface segmentation to define the CSF space and a dural sac with a thickness of 300 μm.[2] Based on average measurements of the dorsal epidural space at the T8-T9 spinal levels in the preoperative MRI, we defined the epidural space as a 2 mm thick layer surrounding the dural sac. We defined the spine as a simple 4 mm thick layer surrounding the epidural space. We defined an additional general thorax layer as a cylinder with a 100 mm diameter that followed the approximate trajectory of the dural sac.

To define the lead array within the FEM, we first generated a 3D object to match the geometry of the Medtronic Model 39565 Specify^{TM} 5-6-5 Surgical Lead array (Medtronic, Inc.). The lead body had a transverse width (mediolateral) of 10 mm, rostrocaudal length of approximately 64 mm, and thickness of 2 mm. The individual electrodes had a length of 4 mm and a width of 1.5 mm (geometric surface area of 6 mm^2). The individual electrodes had longitudinal and lateral (center-to-center) spacings of 9 mm and 3 mm, respectively. We then

coregistered this lead array to the patient-specific electrode locations (i.e. centroid of the leads from the CT artifact) using the 'N-points registration' and 'Global registration' functions in 3-matic.

We then used the 'Create volume mesh' function in 3-matic to convert the 3D surface objects into a 3D FEM. We included a high-node-density ROI that was 80 mm in length and was centered around C7. For the extracellular voltage calculations, we assumed the lead body was a perfect insulator and removed the lead volume from the FEM. The finalized FEM consisted of more than 33 million first-order tetrahedral elements.

Canonical finite element models

To determine the potential significance of accounting for patient-specific anatomy and electrode locations, we also performed model simulations with two versions of a canonical FEM (Fig. S2b). This canonical FEM had an idealized spinal cord anatomy and an idealized lead placement at the spinal cord midline. Idealized canonical FEMs have been used extensively in the literature to investigate potential mechanisms of action of SCS and other technical issues related to the direct neuromodulatory effects of SCS (e.g. stimulation configuration, lead design, pulse width).[2–4]

This canonical FEM consisted of the gray and white matter of the spinal cord, CSF, dura, epidural fat, vertebral bone, and a surrounding general thorax layer. The dimensions of the spinal cord and the white and gray matter boundaries were defined by human cadaver samples of the lower thoracic spinal cord with anteroposterior and mediolateral dimensions of 5 and 7.4 mm, respectively.[1] The FEM also contained an explicit representation of a Medtronic Model 39565 Specify™ 5-6-5 Surgical Lead array implanted in the epidural fat dorsal to the spinal cord. The dorsal CSF layer had a thickness of 3.2 mm, a value within the range clinically observed at the lower thoracic levels.[5] In the first version of the canonical FEM, the lead array was placed directly on the dorsal surface of the dura along the spinal cord midline. In the

second version of the canonical FEM, we developed an “impedance-matched” canonical model by adding a 300 µm thick encapsulation layer domain around the lead body.

The model geometry was defined and meshed in 3-matic. We specified higher mesh densities near the electrode array as well as within a 70 mm long region of interest surrounding the electrode array. The total model length was 201 mm with a diameter of 70 mm. The FEM consisted of more than 2.6 million first-order tetrahedral elements.

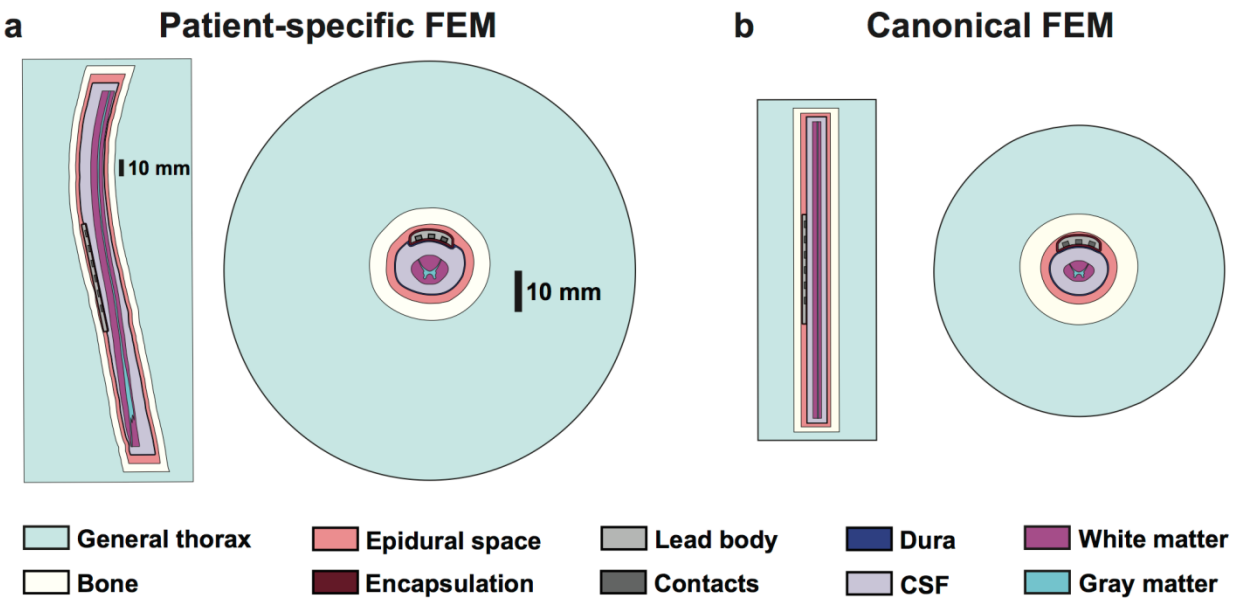

Figure S2. Volume conductor models. Sagittal (left) and axial (right) views of the finite element model (FEM) designs for the (a) patient-specific and (b) canonical models.

Extracellular voltage calculations

To calculate the voltage distributions generated by SCS, we exported the patient-specific and canonical volume meshes generated in 3-matic and imported them into the finite element analysis software package, COMSOL Multiphysics (COMSOL, Inc., Burlington, MA). Within COMSOL, we assigned the appropriate electrical conductivities to each domain based on experimental data available in the literature (Table S1).[3,4,6]

To account for the patient-specific electrode impedances and to represent the electrode encapsulation that occurs with chronic SCS implants,[7] we included a 300 μm thick encapsulation layer domain around the lead body in the patient-specific model and the impedance-matched canonical model. During the research testing, we used the built-in functionality of the IPG to measure the bipolar electrode impedances relative to C0. At the end of the research visit, the electrodes had an average bipolar impedance of 695±34.7 Ω. We used bench testing to determine that this total electrode impedance corresponded to a tissue impedance of 530 Ω.[8,9] In both the patient-specific and the impedance-matched canonical FEMs, we applied the appropriate boundary conditions to each FEM (i.e. 0 V at C0 and 1 V at the individual contact) to simulate the 15 pairs of bipolar electrode impedances and solved each FEM for each pair. We calculated the tissue impedance for each bipolar combination by integrating the total current generated in the FEM for a 1 V stimulus (i.e. $Z_{FEM} = 1\ V / I_{FEM}$). We then averaged the 15 model impedances to calculate the corresponding average FEM tissue impedance. In both the patient-specific and the impedance-matched canonical FEMs, we adjusted the conductivity of the encapsulation layer domain until each FEM produced an average impedance of approximately 530 Ω. We determined that encapsulation layer conductivities of 0.46 and 0.49 S/m produced average FEM tissue impedances of 533 and 531 Ω for the patient-specific and impedance-matched canonical models, respectively (Table S1).

To calculate the extracellular voltages generated during SCS, we applied boundary conditions of 1 V and 0 V at the cathode (C7) and anode(s), respectively, and set the outer tissue boundary to be perfectly insulating. We then solved Laplace's equation to calculate the voltage distributions generated in the tissue for a given stimulation configuration. We calculated the electrostatic FEM solutions for these unit voltages with an iterative equation solver using the conjugate-gradient method. We refined the mesh density until further increasing the mesh density produced a maximum ≤ 4% differences in the activation thresholds calculated for the neural elements considered in this study. The corresponding spatially-dependent FEM voltage

solutions were then scaled by the time-dependent output of the IPG (see below) to determine the spatiotemporal extracellular voltages.

Table S1. Electrical conductivities used in the finite element models

Tissue	Conductivity (S/m)
White matter (longitudinal)	0.600
White matter (transverse)	0.083
Gray matter	0.230
Cerebrospinal fluid	1.700
Dura	0.600
Encapsulation layer (patient-specific model)	0.460
Encapsulation layer (impedance-matched canonical model)	0.490
Epidural fat	0.040
Vertebral bone	0.020
General thorax	0.250

Time-dependent stimulator output

To incorporate accurate time-dependent descriptions of the IPG output, we developed a circuit model to closely mimic the components of the clinical SCS system and the IPG (Fig. S3).[8,9] We represented the electrode-tissue interface (ETI) of the stimulating electrodes via a 3.3 μF capacitor (C_{elec}) based on the surface area of each electrode.[10] We also incorporated 10 μF blocking capacitors (C_{block}) at each output of the RestoreSensor™ IPG,[11] a 15 Ω resistance representing the lead extension (R_{ext}) that connects the IPG to the lead wire, and a 27 Ω resistance representing the lead wire (R_{lead}). The resistance of the lead extension and the lead wire were average resistance values directly measured from an extension model 7483 and a

Model 39565 Specify™ 5-6-5 Surgical Lead (Medtronic, Inc.), respectively. We specified R_{tissue} to achieve the desired tissue impedance determined from the FEM. For example, for a stimulation configuration of C7(-) and C8(+), the patient-specific FEM had a tissue impedance of 503 Ω. Therefore, we defined R_{tissue} as 503 Ω to estimate the time-dependent V_{tissue} waveform for a bipolar stimulation configuration of C7(-) and C8(+). For stimulation configurations with multiple anodes, we added additional branches to the bottom of the circuit shown in Fig. S3 using the same values for C_{elec}, R_{lead}, R_{ext}, and C_{block}. This method assumed that the voltage stimulus resulted in equal currents through each anodic branch. We repeated this process for all stimulation configurations that we considered in this study. The IPG model also included two switches, one switch to apply the cathodic stimulus pulse and the second switch to allow for passive discharging.

To accurately reproduce the IPG output, it was important to understand the output modes of the IPG. During the cathodic stimulus pulse, the IPG applied the selected pulse amplitude across the entire IPG circuit. At the end of the cathodic pulse, the circuit was placed in a “high-impedance” state that mimicked an open circuit for 80 μs to allow for more efficient neural excitation.[12] At the end of this 80 μs interphase interval, residual charge in the IPG circuit was allowed to passively discharge. This passive discharge phase allowed for charge accumulated across the ETI capacitance and blocking capacitors to discharge. The duration of this passive discharge phase was dependent on the pulse frequency and pulse width and was 19.6 ms for a pulse frequency of 50 Hz and a pulse width of 300 μs. At the end of the passive discharge phase, the IPG was placed in a “high-impedance” state until the start of the next cathodic stimulus pulse.

To calculate the time-dependent tissue voltage (V_{tissue}), we first defined the desired V_{stim} waveform in the time domain using the desired pulse width, pulse frequency of 50 Hz, pulse amplitude of 1 V, and a sampling frequency of 500 kHz. We then accounted for the filtering effects of the circuit in the frequency domain using the appropriate transfer function to estimate

the circuit output, V_{tissue}. We then inversed transformed the output to obtain the time-dependent V_{tissue} waveform. We calculated the corresponding time-dependent V_{tissue} for each circuit design and set of stimulation parameters (Fig. S3). V_{tissue} represented the input to our 3D FEM analysis.

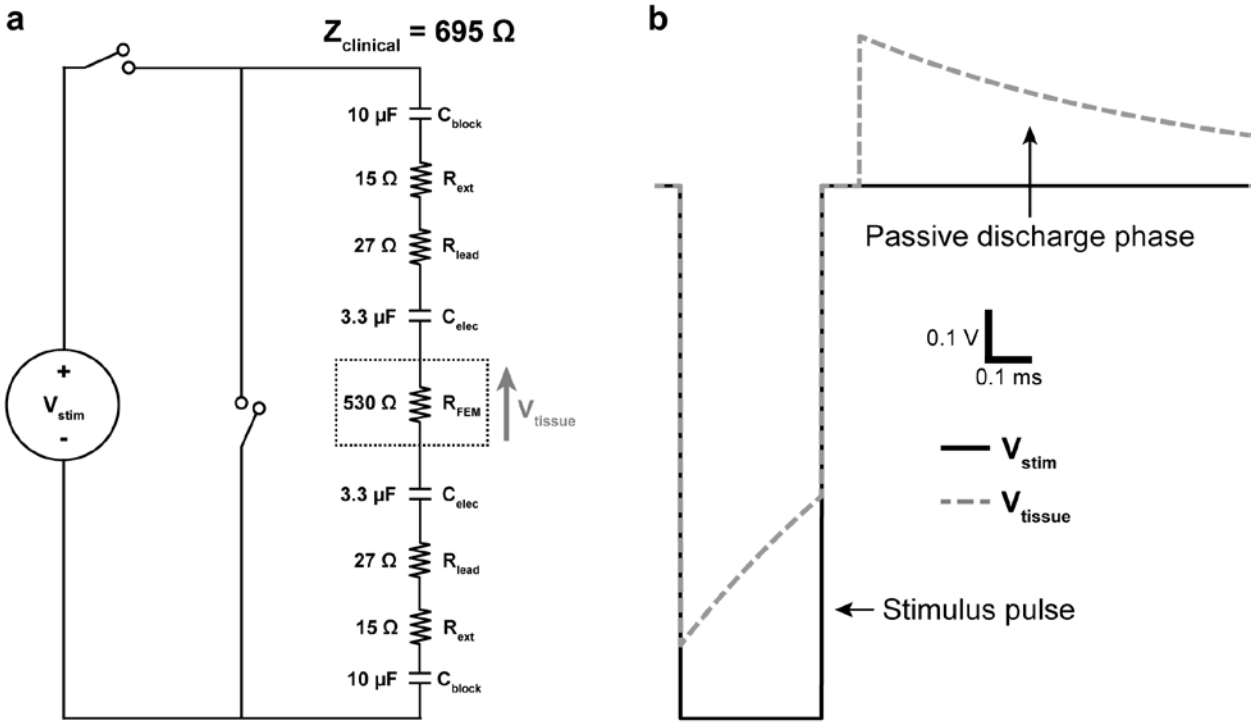

Figure S3. Circuit model to describe the time-dependent output of the SCS IPG. a. The IPG circuit model included the blocking capacitors on the IPG outputs (C_{block}), resistance of the SCS extension wires (R_{ext}), resistance of the SCS lead wires (R_{lead}), and the capacitance of the electrode-tissue interface (C_{elec}). This model also included two switches. The top-left switch closed to apply the cathodic pulse while the lower-right switch closed to allow for passive discharging. b. Computer simulation of the time-dependent tissue voltage (V_{tissue}) using the following stimulation parameters: pulse amplitude (i.e. V_{stim}) = 1 V, pulse width = 300 μs, and pulse frequency = 50 Hz.

Axon models

We represented the spinal cord and dorsal root (DR) fibers with a previously published compartmental model of a mammalian motor axon.[13] This model reproduces experimental data by accurately representing the ion channels at the nodes of Ranvier as well as matching the geometry of the paranode, internode, and myelin to measured morphology. This model incorporates a double-layer cable model that accounts for the finite impedance of the myelin sheath. The nodes of Ranvier contain fast Na^+, persistent Na^+, and slow K^+ nonlinear conductances as well as the linear leakage conductance and the membrane capacitance.

We generated populations of spinal cord axons that mimicked the range of axon diameters and densities measured within the human spinal cord. We calculated the relative densities of each axon diameter from histograms of myelinated axon populations within the superficial dorsal column of the human spinal cord.[14] We first divided the histograms into the discrete axon diameters that were available for the given axon model (i.e. 5.7, 7.3, 8.7, 10.0, 11.5, 12.8, 14.0, 15.0, 16.0 μm).[13] Second, we normalized the histogram to determine the percentage of axons within each specified diameter range. Third, to calculate the density of axons for a given diameter, we multiplied the percentage of axons by the total density of axons per area (i.e. 22.92 axons/1000 μm^2).[14] Finally, to determine the total number of axons for a given diameter, we then multiplied the individual axon density by the total cross section area of the white matter areas within the spinal cord. We repeated these steps for each axon diameter. For computational simplicity, we only used 1% of the true anatomical densities. In our analyses, we did not include axon diameters < 5.7 μm because they were unlikely to be excited by SCS[4] or axon diameters > 11.5 μm due to their relatively low density within the spinal cord.[14] We used Lloyd's algorithm with 10,000 iterations to uniformly distribute each axon population within the white matter of the spinal cord.[15]

For the patient-specific model, spinal cord axons with a diameter of 5.7, 7.3, 8.7, 10.0, and 11.5 μm had a length of 199, 199, 199, 199, and 199 mm and 399, 266, 200, 174, and 160

nodes of Ranvier, respectively. The patient-specific model had 1882, 1232, 468, 142, and 37 axons for diameters of 5.7, 7.3, 8.7, 10.0, and 11.5 μm, respectively, corresponding to a total of 3761 axons (1427 axons within the dorsal columns (DC)). For both versions of the canonical model, spinal cord axons with a diameter of 5.7, 7.3, 8.7, 10.0, and 11.5 μm had a length of 160, 160, 159, 160, and 159 mm and 320, 214, 160, 140, and 128 nodes of Ranvier, respectively. The canonical models had 1167, 761, 285, 86, and 22 axons for diameters of 5.7, 7.3, 8.7, 10.0, and 11.5 μm, respectively, corresponding to a total of 2321 axons (783 axons within the DC). For the patient-specific model, the mother DR fiber had a diameter of 8.7 μm and a length of 56 mm with 56 nodes of Ranvier. The daughter DC fiber had a diameter of 7.3 μm and a length of 198 mm with 265 nodes of Ranvier. For both versions of the canonical model, the mother DR fiber had a diameter of 8.7 μm and a length of 44 mm with 44 nodes of Ranvier. The daughter DC fiber had a diameter of 7.3 μm and a length of 160 mm with 214 nodes of Ranvier. The patient-specific and canonical models included 102 DR fibers. Simulations were performed with the software package, NEURON, within the Python programming environment.[16] Model solutions were calculated using backward Euler implicit integration with a time step of 0.002 ms.

Simulation procedures

To assess the direct axonal response to SCS, we ported the spatiotemporal 3D voltage distributions calculated in the FEM and the IPG circuit model to the Python programming environment and directly applied the voltage distributions to the axon models of the DC and DR fibers. Because the bulk conductivity was linear, the voltage distributions generated by the different stimulation waveforms were scaled versions of the original FEM solutions with a unit voltage. We interpolated the scaled voltage distributions onto the model axons described above using the extracellular mechanism within NEURON. We determined the activation thresholds for each axon using a bisection algorithm (error < 0.1 V).

REFERENCES

1. Kameyama T, Hashizume Y, Sobue G. Morphologic Features of the Normal Human Cadaveric Spinal Cord. *Spine (Phila Pa 1976)*. 1996;21(11):1285-1290.
2. Lempka SF, McIntyre CC, Kilgore KL, Machado AG. Computational Analysis of Kilohertz Frequency Spinal Cord Stimulation for Chronic Pain Management. *Anesthesiology*. 2015;122(6):1362-1376. doi:10.1097/ALN.0000000000000649.
3. Lee D, Hershey B, Bradley K, Yearwood T. Predicted effects of pulse width programming in spinal cord stimulation: a mathematical modeling study. *Med Biol Eng Comput*. 2011;49(7):765-774. doi:10.1007/s11517-011-0780-9.
4. Holsheimer J. Which neuronal elements are activated directly by spinal cord stimulation. *Neuromodulation*. 2002;5(1):25-31. doi:10.1046/j.1525-1403.2002._2005.x.
5. Holsheimer J, den Boer JA, Struijk JJ, Rozeboom AR. MR Assessment of the Normal Position of the Spinal Cord in the Spinal Canal. *AJNR Am J Neuroradiol*. 1994;15(5):951-959.
6. Ladenbauer J, Minassian K, Hofstoetter US, Dimitrijevic MR, Ratty F. Stimulation of the Human Lumbar Spinal Cord With Implanted and Surface Electrodes - A Computer Simulation Study. *IEEE Trans Neural Syst Rehabil Eng*. 2010;18(6):637-645.
7. Arle JE, Carlson KW, Mei L, Shils JL. Modeling Effects of Scar on Patterns of Dorsal Column Stimulation. *Neuromodulation*. 2014;17(4):320-333. doi:10.1111/ner.12128.
8. Gunalan K, Chaturvedi A, Howell B, et al. Creating and parameterizing patient-specific deep brain stimulation pathway-activation models using the hyperdirect pathway as an example. *PLoS One*. 2017;12(4):e0176132.
9. Lempka SF, Howell B, Gunalan K, Machado AG, McIntyre CC. Characterization of the stimulus waveforms generated by implantable pulse generators for deep brain stimulation. *Clin Neurophysiol*. 2018;129(4):731-742. doi:10.1016/j.clinph.2018.01.015.

10. Butson CR, McIntyre CC. Tissue and electrode capacitance reduce neural activation volumes during deep brain stimulation. *Clin Neurophysiol*. 2005;116(10):2490-2500. doi:10.1016/j.clinph.2005.06.023.

11. Liu X, Demostheous A, Donaldson N. Five valuable functions of blocking capacitors in stimulators. In: *13th Annual Conference of the International Functional Electrical Stimulation Society*. ; 2008:322-324.

12. van den Honert C, Mortimer JT. The response of the myelinated nerve fiber to short duration biphasic stimulating currents. *Ann Biomed Eng*. 1979;7(2):117-125.

13. McIntyre CC, Richardson AG, Grill WM. Modeling the Excitability of Mammalian Nerve Fibers: Influence of Afterpotentials on the Recovery Cycle. *J Neurophysiol*. 2002;87:995-1006.

14. Feirabend HKP, Choufoer H, Ploeger S, Holsheimer J, van Gool JD. Morphometry of human superficial dorsal and dorsolateral column fibres: significance to spinal cord stimulation. *Brain*. 2002;125:1137-1149.

15. Lloyd SP. Least Squares Quantization in PCM. *IEEE Trans Inf Theory*. 1982;IT-28(2):129-137.

16. Hines ML, Andrew P, Muller E. NEURON and Python. *Front Neuroinform*. 2009;3(January):1-12. doi:10.3389/neuro.11.001.2009.

Table 1. Clinical and model-based sensory thresholds.

		Clinical ST	Patient-specific model ST	Canonical model ST	Impedance-matched canonical ST
Pulse width	60	6.6	7.5	3.9	5.8
	210	3.3	3.1	1.6	2.4
	300	2.7	2.6	1.4	2.0
	450	2.5	2.3	1.3	1.7
	1000	1.9	2.1	1.2	1.6
	MAPE		8.9%	44.9%	22.0%
Stimulation configuration	Bipole	2.7	2.6	1.4	2.0
	Longitudinal tripole	2.2	2.0	1.0	1.5
	Transverse tripole	3.3	2.4	1.2	1.8
	Pseudo-monopole	2.9	3.1	1.7	2.4
	MAPE		12.1%	51.1%	30.8%

ST = sensory threshold; MAPE = mean absolute percentage error.